

Testing Weyl geometric gravity with the SPARC galactic rotation curves database

Maria Crăciun^a, Tiberiu Harko^{b,c,d,*}

^a'Tiberiu Popoviciu' Institute of Numerical Analysis, Romanian Academy, 57, Fantanele Street, Cluj-Napoca, 400320, Cluj, Romania

^bDepartment of Theoretical Physics, National Institute of Physics and Nuclear Engineering (IFIN-HH), , Bucharest, 077125, , Romania

^cDepartment of Physics, Babes-Bolyai University, Kogalniceanu Street, Cluj-Napoca, 400084, Cluj, Romania

^dAstronomical Observatory, Romanian Academy, 19 Ciresilor Street, Cluj-Napoca, 400487, Cluj, Romania

Abstract

We present a detailed investigation of the properties of the galactic rotation curves in the Weyl geometric gravity model, in which the gravitational action is constructed from the square of the Weyl curvature scalar, and of the strength of the Weyl vector. The theory admits a scalar-vector tensor representation, obtained by introducing an auxiliary scalar field. By assuming that the Weyl vector has only a radial component, an exact solution of the field equations can be obtained, which depends on three integration constants, and, as compared to the Schwarzschild solution, contains two new terms, linear and quadratic in the radial coordinate. In the framework of this solution we obtain the exact general relativistic expression of the tangential velocity of the massive test particles moving in stable circular orbits in the galactic halo. We test the theoretical predictions of the model by using 175 galaxies from the Spitzer Photometry & Accurate Rotation Curves (SPARC) database. We fit the theoretical predictions of the rotation curves in conformal gravity with the SPARC data by using the Multi Start and Global Search methods. In the total expression of the tangential velocity we also include the effects of the baryonic matter, and the mass to luminosity ratio. Our results indicate that the simple solution of the Weyl geometric gravity can successfully account for the large variety of the rotation curves of the SPARC sample, and provide a satisfactory description of the particle dynamics in the galactic halos, without the need of introducing the elusive dark matter particle.

Keywords: dark matter, Weyl geometric gravity, SPARC database, galactic rotation curves

PACS: 04.50.Kd, 04.20.Cv

Contents

1 Introduction	1	4.3 Fitting results	8
2 Essentials of Weyl geometry, and of Weyl geometric gravity	4	4.4 Fitting results for galaxies without bulge velocity information	8
2.1 Weyl geometry	4	4.5 Correlations of the optimal parameters	10
2.2 Weyl geometric gravity-action and field equations	4	4.6 Fitting of the galaxies with bulge velocity data	10
3 Exact static analytical solution and the tangential rotation curves in Weyl geometric gravity	5	4.7 Optimal parameters distribution	17
3.1 Exact solution of the Weyl geometric gravity field equations	5	4.8 Correlations between the parameters of the model, and the astrophysical quantities	17
3.2 Rotational velocities in static spherically symmetric geometries	6		
3.3 Tangential velocity in Weyl geometric gravity	7		
4 Fitting the Weyl geometric rotation curves with the SPARC sample	7	5 Discussions and final remarks	18
4.1 The SPARC dataset	7		
4.2 Material and methods	8	1. Introduction	
4.2.1 The theoretical model	8		
4.2.2 The fitting procedure	8		

*Corresponding author.

Email address: tiberiu.harko@aira.astro.ro (Tiberiu Harko)

$\sigma_8 = 0.811 \pm 0.006$ [1], respectively. Hence, baryonic matter constitutes only around 17% of the total mass budget in the Universe, the rest of the matter being in the form of dark matter.

Dark matter resides in large halos around the visible baryonic matter distribution in galaxies, and its existence is inferred from two important observational evidences: the behavior of the galactic rotation curves, and the mass deficit in clusters of galaxies.

Despite its remarkable success in explaining cosmological observations, the Λ CDM model is facing several important challenges when trying to explain the astrophysical properties of the galaxies, and of their dark matter halos. The discrepancies between theory and observations become more important for the dwarf galaxies, with the Λ CDM theoretical predictions for the number, spatial distribution, and internal structure of low-mass dark-matter halos being contradicted by the observed properties of dwarf galaxies [2]. One of these problems is the core-cusp problem, which originated in the numerical simulations suggesting dark matter densities diverging as $\rho \propto r^{-1}$ in the inner regions of the halo [3]. On the other hand, observations of the rotation curves in some dwarf galaxies indicate that their inner densities are consistent with a constant-density core [4]. This problem can be solved by assuming, for example, that dark matter is in the form of a Bose-Einstein Condensate [5–7].

A persistent, and a yet unsolved challenge to the Λ CDM model is the observed diversity of the rotation curves [2]. The observed rotation curves of different types of galaxies show a wide range of forms. Even the rotation curves have a similar outer behavior, their inner behavior is still very different. Simulations of baryonic matter could not consistently describe the different velocity curve shapes in the inner regions of the galaxies [2].

Up to now, the only evidence for the existence of dark matter is only gravitational, and no experimental detection of any dark matter particle has been reported yet. Hence, the problem of the reality of the dark matter particle is still open, and the existence of alternative explanations for the observational data cannot be excluded a priori. One of the possible solutions for the understanding of the galactic dynamics may be obtained by assuming that dark matter is just a modification of the gravitational force at galactic or extra-galactic scales. Hence, beyond the boundaries of the Solar System, the Newtonian or general relativistic laws of gravity are naturally modified, and the gravitational phenomena are described by a new, fundamental theory of gravity.

The behavior of the rotation curves may be thus explained by modifying the laws of Newtonian physics, as done is the MOND (Modified Newtonian Dynamics) theory [8]. Modified theories of gravity have been extensively applied to look for possible explanations of the dark matter related phenomenology [9–24]. For example, in [13] it was shown that a slight modification of the Einstein-Hilbert Lagrangian of the form $R^{1+\delta}$, $\delta \ll 1$, could explain the behavior of the galactic rotation curves without postulating the existence of dark matter. A detailed review of the dark matter problem in modified theories of gravity with geometry-matter coupling is presented in [25]. For a review of the particle physics aspects of dark matter

see [26].

In 1918, a few years after the proposal of general relativity, Weyl [27, 28] introduced a generalization of Riemann geometry, based on the idea of the conformal invariance of the physical laws. Weyl’s main goal was to obtain a unified theory of gravitation and electromagnetism. Even as a unified field theory Weyl’s approach is no longer seen as valid, the geometrical (and physical) ideas he introduced represent an attractive theoretical framework, on which extensions of general relativity can be constructed. For detailed presentation of the role of Weyl geometry in physics see [29]. Gravitational theories derived from Weyl geometry are pure metric, and they contain the equivalence principle, as well as the general covariance principle of general relativity. Moreover, a supplementary symmetry, local conformal invariance, is added in a nontrivial way to the theory, by requiring that the action is invariant with respect to local conformal transformations of the metric given by $g_{\mu\nu}(x) \rightarrow e^{2\omega(x)}g_{\mu\nu}(x)$, where the local phase $\omega(x)$ is an arbitrary function of the coordinates. Moreover, Weyl’s geometry is non-metric, and has the basic property that the covariant divergence of the metric is nonzero. This property also leads to the existence of a specific Weyl connection, which generalizes the Levi-Civita connection of Riemannian geometry. For a discussion between the differences between the notions of conformal and Weyl invariance see [30].

One of the modified theories of gravity in which the galactic rotation curves have been extensively investigated is the conformal Weyl gravity [31–36]. This modified gravity theory is built on the principle of local conformal invariance, which severely restricts the choice of the action for the gravitational field, by requiring that the action remains invariant under any conformal transformation $g_{\mu\nu} \rightarrow \Omega(x)g_{\mu\nu}$ of the metric. One of the simplest possibilities to satisfy the principle of the covariant invariance is to construct the action from the conformally invariant Weyl tensor $C_{\mu\nu\rho\kappa}$ [31]. Once the conformal invariance is strictly imposed, particle masses can only be generated through the spontaneous breaking of the symmetry of the action. The complete, exact exterior solution for a static, spherically symmetric object in conformal Weyl gravity was found in [31]. The solution contains as a particular case the Schwarzschild solution of general relativity, and also contains in the metric a new term that grows linearly with distance. It was suggested in [31] that this solution could provide an explanation for the observed galactic rotation curves, without the requiring the existence of dark matter. This interesting idea was further investigated through a detailed comparison of the theoretical solution with the observations [37–41].

The contributions of the Weyl gravity approach to the galactic dynamics can be summarized as follows. There are two new effects that do appear on galactic and extra-galactic scales, leading to a modification of the Newtonian gravity. Locally, the baryonic matter sources within galaxies generate not only Newtonian potentials, but also linear potentials. Globally, two new potentials, one linear, and the other one quadratic, are created by the rest of the ordinary matter in the Universe [37]. The universal linear potential term has the form $V(r) = \gamma_0 c^2 r/2$, where γ_0 is a constant, and it can be associated with the cosmic back-

ground itself. The second, de Sitter type universal potential, is taken as $V(r) = -\kappa c^2 r^2/2$, and it is induced by the inhomogeneities in the Cosmic Microwave Background Radiation [37]. In [38] Weyl gravity theory was applied to a sample of 111 spiral galaxies, consisting of high surface brightness galaxies, low surface brightness galaxies, and dwarf galaxies, respectively, having rotation curve data points extending beyond the optical disk. By considering as free parameters only the galactic mass-to-light ratios, the theory can describe the properties of this set of rotation curves without the need for invoking the presence of dark matter. The investigations initiated in [38] were extended in [39] by considering a supplementary set of 27 galaxies, of which 25 are dwarf galaxies, plus 3 additional galaxies belonging to the original sample. Fully acceptable fits were found for this sample, thus bringing to 138 the number of rotation curves of galaxies that could be explained in the conformal gravity theory. These studies seem also to confirm the idea that dark matter is just a universal contribution to galactic dynamics, originating from matter located outside of the galaxies, and thus independent of them.

On the other hand, in [42] it was shown that in conformally invariant gravity theories, defined on Riemannian spacetimes, and having the Schwarzschild - de Sitter metric as a solution of the Einstein field equations, the trajectories followed by baryonic matter particles are the timelike geodesics of the Schwarzschild-de Sitter metric, thus leading to rotation curves with no flat regions. Moreover, attempts to model rising rotation curves by fitting the coefficient of the quadratic term for each independent galaxy cannot be successful, since this term can be interpreted as a (very small) cosmological constant Λ . Moreover, it was shown that the invariance of particle dynamics with respect to the choice of the conformal frame is also valid for arbitrary metrics. The same results apply for conformally invariant gravity theories constructed in more general Riemann-Weyl-Cartan spacetimes. The above results can be illustrated as follows. In the case of a static spherically symmetric metric with $g_{00} = 1/g_{11} = 1 - 2GM/R - kr^2$, the tangential velocity of massive particles can be obtained as $v^2 = (GM/r - kr^2) / (1 - 2GM/r - kr^2)$. Since in the Newtonian limit the two terms in the numerator dominate, we obtain $v^2 = v_{Kep}^2 - kr^2$, where $v_{Kep}^2 = GM/r$. By assuming $k = \Lambda/3$, with $\Lambda = 10^{-52} \text{ m}^{-2}$, for a galaxy of mass $M \sim 10^{11} M_\odot$, the rotation curve will fall for all r until the circular orbits become unbounded at a radius $r = (3GM/\Lambda c^2)^{1/3} \sim 0.5 \text{ Mpc}$ [42]. Hence, it turns out that the rotation curves do not have a flat region.

An interesting perspective on Weyl geometry, and its physical applications was recently introduced in [43–52]. The basic, and novel idea, is to linearize in the curvature scalar the conformally invariant quadratic Weyl action by introducing an auxiliary scalar field. Hence, the initial purely vector-tensor gravity is transformed into a scalar-vector-tensor theories, which has many attractive features. In its linear representation in Weyl quadratic gravity a spontaneous breaking of the D(1) symmetry takes place, triggered by a Stueckelberg type type, mechanism. As a result, the Weyl gauge field acquires mass from the spin-

zero mode of the \tilde{R}^2 term in the action. Through this mechanism, from the Weyl action the Einstein-Proca Lagrangian is reobtained, after the elimination of the auxiliary scalar field. The Planck scale is generated from the scalar field mode, and, moreover, the cosmological constant also emerges in the broken phase. It also turns out that all the mass scales, like the Planck scale, the cosmological constant, and the Higgs field originate from geometry [50], with the Higgs field generated by the fusion of Weyl bosons in the early Universe

Various astrophysical and cosmological implications of the scalar-vector-tensor Weyl theory, also called Weyl geometric gravity, have been investigated in [53–58]. Black hole solutions in Weyl geometric gravity have been studied numerically in [55], where an exact solution of the field equations has also been obtained, corresponding to a specific choice, and form, of the Weyl vector. This solution is mathematically similar to the exact solution of the conformal Weyl gravity [31], but its physical meaning, origin and interpretation are different. The possibility that this solution, extended to galactic scales, may account for the description of the behavior of the galactic rotation curves was suggested in [56], where a small sample of seven galaxies was used to fit the Weyl geometric theoretical model with the observations.

It is the goal of the present paper to continue, and extend the investigation initiated in [56] by considering a full comparison of the simple three-parameter Weyl geometric dark matter model with the rotation curves data of the SPARC dataset. The SPARC (Spitzer Photometry & Accurate Rotation Curves) database [59, 60] consists of a sample of 175 nearby galaxies, with surface photometry at $3.6 \mu\text{m}$. It also contains high-quality rotation curves, obtained from HI/H α data. SPARC covers a large range of galactic morphologies, ranging from S0 to Irr, galactic luminosities (5 dex), as well as surface brightnesses at 4 dex. Galactic mass models based on SPARC data have also been constructed, and with their help the ratio (V_{bar}/V_{obs}) of baryonic-to-observed velocity has been quantitatively estimated for different characteristic galactic radii, and various values at [3.6] of the stellar mass-to-light ratio (M/L) [59, 60]. The SPARC database was extensively used to analyze different dark matter models, and to obtain constraints on the model parameters [61–70].

In order to perform the comparison between the model and the observations we obtain first the full general relativistic expression of the tangential velocity of massive test particles moving in stable circular orbits. In total velocity of the particles we include, together with the Weyl contribution, the effects of the different components of the baryonic matter, together with their corresponding mass to light ratios. Our results indicate that the Weyl geometric gravity dark matter model could offer a satisfactory explanation of galactic dynamics without invoking the need of the existence of dark matter.

The present paper is organized as follows. We briefly review the basic concepts and ideas of Weyl geometry and of Weyl geometric gravity in Section 2. We present the derivation of the exact solution of the static, spherically symmetric field equations of Weyl geometric gravity in Section 3, where also the expression of the tangential velocity in the considered metric is

given, and its properties are discussed. The results of the fitting of the SPARC data with the theoretical model are presented in Section 4, where we also discuss the correlations between the parameters of the model and different astrophysical quantities. Finally, we discuss and conclude our results in Section 5.

2. Essentials of Weyl geometry, and of Weyl geometric gravity

In the present Section we very succinctly present the fundamentals of the Weyl geometry. Then, we introduce the basic, conformally invariant Weyl action, and we present its linearization in the curvature scalar with the use of an auxiliary scalar field, thus transforming the initial vector-tensor theory into a scalar-vector tensor theory. The full set of field equations of the Weyl geometric gravity theory, obtained by varying the action with respect to the metric, is also written down.

2.1. Weyl geometry

Weyl geometry is based on two fundamental ideas. The first important property of Weyl geometry is that the length of a vector is allowed to vary during parallel transport. Hence, the length l of an arbitrary vector parallelly transported from the point x^μ to the infinitesimally closed point $x^\mu + \delta x^\mu$, the length of a vector changes according to the rule

$$\delta l = l\omega_\mu \delta x^\mu, \quad (1)$$

where by ω_μ we have denoted the Weyl vector field. Moreover, Weyl geometry has a second important property, namely, the extension of the metricity condition $\nabla_\alpha g_{\mu\nu} = 0$ of the Riemannian geometry. In Weyl geometry one introduces a new fundamental geometric quantity, called the nonmetricity $Q_{\lambda\mu\nu}$ and defined with the help of the covariant derivative of the metric tensor, given by

$$\tilde{\nabla}_\lambda g_{\mu\nu} = -\alpha\omega_\lambda g_{\mu\nu} \equiv Q_{\lambda\mu\nu}, \quad \tilde{\nabla}_\lambda g^{\mu\nu} = \alpha\omega_\lambda g^{\mu\nu}. \quad (2)$$

where the constant α denotes the Weyl gauge coupling constant. The Weyl connection $\tilde{\Gamma}_{\mu\nu}^\lambda$ can be obtained from the nonmetricity condition (2) as

$$\tilde{\Gamma}_{\mu\nu}^\lambda = \Gamma_{\mu\nu}^\lambda + \frac{1}{2}\alpha\left[\delta_\mu^\lambda\omega_\nu + \delta_\nu^\lambda\omega_\mu - g_{\mu\nu}\omega^\lambda\right] = \Gamma_{\mu\nu}^\lambda + \Psi_{\mu\nu}^\lambda, \quad (3)$$

where $\Gamma_{\mu\nu}^\lambda$ is the Levi-Civita connection of the metric $g_{\mu\nu}$

$$\Gamma_{\mu\nu}^\lambda = \frac{1}{2}g^{\lambda\sigma}\left(\partial_\nu g_{\sigma\mu} + \partial_\mu g_{\sigma\nu} - \partial_\sigma g_{\mu\nu}\right). \quad (4)$$

In the following the geometrical and physical quantities in Weyl geometry will be denoted by a tilde. From the contraction of Eq. (3) we obtain

$$\omega_\mu = \frac{1}{2\alpha}\left(\tilde{\Gamma}_\mu - \Gamma_\mu\right), \quad (5)$$

which gives the geometrical interpretation of the Weyl vector as the difference of the Weyl and Levi-Civita connections.

A geometrical quantity playing an important role in many applications is the field strength $F_{\mu\nu}$ of the Weyl vector ω_μ , is defined according to,

$$\tilde{F}_{\mu\nu} = \tilde{\nabla}_{[\mu}\omega_{\nu]} = \nabla_{[\mu}\omega_{\nu]} = \partial_{[\mu}\omega_{\nu]} = \partial_\mu\omega_\nu - \partial_\nu\omega_\mu. \quad (6)$$

The action of the covariant derivative commutators on vectors and covectors is expressed as

$$\left(\tilde{\nabla}_\mu\tilde{\nabla}_\nu - \tilde{\nabla}_\nu\tilde{\nabla}_\mu\right)v^\sigma = \tilde{R}^\sigma{}_{\rho\mu\nu}v^\rho, \quad (7a)$$

$$\left(\tilde{\nabla}_\mu\tilde{\nabla}_\nu - \tilde{\nabla}_\nu\tilde{\nabla}_\mu\right)v_\sigma = -\tilde{R}^\rho{}_{\sigma\mu\nu}v_\rho. \quad (7b)$$

where we have introduced the Weyl curvature tensor $\tilde{R}_{\mu\nu}^\lambda$ defined according to the definition

$$\tilde{R}_{\mu\nu}^\lambda = \partial_\nu\tilde{\Gamma}_{\mu\sigma}^\lambda - \partial_\sigma\tilde{\Gamma}_{\mu\nu}^\lambda + \tilde{\Gamma}_{\rho\nu}^\lambda\tilde{\Gamma}_{\mu\sigma}^\rho - \tilde{\Gamma}_{\rho\sigma}^\lambda\tilde{\Gamma}_{\mu\nu}^\rho, \quad (8)$$

The Weyl curvature tensor has the symmetry properties

$$\tilde{R}_{\mu\nu\rho\sigma} = -\tilde{R}_{\mu\nu\sigma\rho}, \quad (9)$$

$$\tilde{R}_{\mu\nu\rho\sigma} = -\tilde{R}_{\nu\mu\rho\sigma} + \alpha g_{\mu\nu}F_{\rho\sigma}, \quad (10)$$

$$\begin{aligned} \tilde{R}_{\mu\nu\rho\sigma} &= \tilde{R}_{\rho\sigma\mu\nu} + \frac{\alpha}{2}\left(g_{\mu\nu}F_{\rho\sigma} - g_{\rho\sigma}F_{\mu\nu}\right. \\ &\quad \left.+ g_{\nu\sigma}F_{\mu\rho} - g_{\nu\rho}F_{\mu\sigma} + g_{\mu\rho}F_{\nu\sigma} - g_{\mu\sigma}F_{\nu\rho}\right), \end{aligned} \quad (11)$$

$$\tilde{R}_{\mu\nu} = \tilde{R}_{\nu\mu} + 2\alpha F_{\mu\nu}. \quad (12)$$

The first and the second contractions of the Weyl curvature tensor are given by

$$\tilde{R}_{\mu\nu} = \tilde{R}^\lambda{}_{\mu\lambda\nu}, \quad \tilde{R} = g^{\mu\sigma}\tilde{R}_{\mu\sigma}. \quad (13)$$

Thus we obtain for the Weyl scalar \tilde{R} the expression

$$\tilde{R} = R - 3\alpha\nabla_\mu\omega^\mu - \frac{3}{2}(\alpha)^2\omega_\mu\omega^\mu, \quad (14)$$

where R is the Ricci scalar obtained with the help of the Levi-Civita connection of the Riemannian geometry.

With respect to a conformal transformation with a conformal factor $\Sigma(x)$, the variations of the metric tensor, of the Weyl field, and of a scalar field ϕ are given by

$$\tilde{g}_{\mu\nu} = \Sigma^2(x)g_{\mu\nu}, \quad \tilde{\omega}_\mu = \omega_\mu - \frac{2}{\alpha}\partial_\mu \ln \Sigma(x), \quad \tilde{\phi} = \Sigma^{-1}(x)\phi. \quad (15)$$

2.2. Weyl geometric gravity-action and field equations

The simplest gravitational Lagrangian density in Weyl geometry, which is conformally invariant, was first considered by Weyl [27–29], and can be defined according to [45–49]

$$\tilde{L}_{Weyl} = \left[\frac{1}{4!}\frac{1}{\xi^2}\tilde{R}^2 - \frac{1}{4}\tilde{F}_{\mu\nu}^2\right]\sqrt{-g}, \quad (16)$$

where $\xi < 1$ denotes the parameter of the perturbative coupling. We will linearize the Lagrangian \tilde{L}_{Weyl} in the curvature by introducing the scalar field ϕ_0 according to the definition [45–49]

$$\tilde{R}^2 \rightarrow 2\phi_0^2\tilde{R} - \phi_0^4, \quad (17)$$

The new Lagrangian density obtained after this substitution is equivalent mathematically to the original one. This result follows from the use of the solution of the equation of motion of ϕ_0 , $\phi_0^2 = \tilde{R}$ in the new Lagrangian \tilde{L}_{Weyl} . Hence, via this substitution, we obtain a new geometric Lagrangian, defined in Weyl geometry, which includes a scalar degree of freedom, and is given by

$$\tilde{L}_{Weyl} = \sqrt{-g} \left[\frac{1}{12} \frac{1}{\xi^2} \phi_0^2 \tilde{R} - \frac{1}{4} \tilde{F}_{\mu\nu}^2 - \frac{\phi_0^4}{4! \xi^2} \right]. \quad (18)$$

The Lagrangian (18) gives the simplest gravitational Lagrangian density fully including the Weyl gauge symmetry, since it is conformally invariant. \tilde{L}_{Weyl} contains a spontaneous breaking of the conformal symmetry, which leads to an Einstein-Proca Lagrangian for ω_μ .

To obtain the gravitational action of Weyl geometric gravity we substitute in Eq. (18) \tilde{R} by its expression given by Eq. (14). Then, after a gauge transformation, and by redefining the geometrical and physical quantities, we find the Riemann space action of Weyl geometric gravity, given by [45–47]

$$\mathcal{S}_{Weyl} = \int d^4x \sqrt{-g} \left[\frac{1}{12} \frac{\phi^2}{\xi^2} (R - 3\alpha \nabla_\mu \omega^\mu - \frac{3}{2} \alpha^2 \omega_\mu \omega^\mu) - \frac{1}{4!} \frac{\phi^4}{\xi^2} - \frac{1}{4} \tilde{F}_{\mu\nu} \tilde{F}^{\mu\nu} \right], \quad (19)$$

The action \mathcal{S}_{Weyl} is fully invariant under conformal transformations.

By varying the action (19) with respect to the metric tensor we obtain the field equations of Weyl geometric gravity as [55, 56],

$$\begin{aligned} & \frac{\phi^2}{\xi^2} (R_{\mu\nu} - \frac{1}{2} R g_{\mu\nu}) + \frac{1}{\xi^2} (g_{\mu\nu} \square - \nabla_\mu \nabla_\nu) \phi^2 \\ & - \frac{3\alpha}{2\xi^2} (\omega^\rho \nabla_\rho \phi^2 g_{\mu\nu} - \omega_\nu \nabla_\mu \phi^2 - \omega_\mu \nabla_\nu \phi^2) \\ & + \frac{3\alpha^2}{4\xi^2} \phi^2 (\omega_\rho \omega^\rho g_{\mu\nu} - 2\omega_\mu \omega_\nu) - 6\tilde{F}_{\rho\mu} \tilde{F}_{\sigma\nu} g^{\rho\sigma} \\ & + \frac{3}{2} \tilde{F}_{\rho\sigma}^2 g_{\mu\nu} + \frac{1}{4\xi^2} \phi^4 g_{\mu\nu} = 0. \end{aligned} \quad (20)$$

The trace of Eq. (20) gives

$$\Phi R + 3\alpha \omega^\rho \nabla_\rho \Phi - \Phi^2 - \frac{3}{2} \alpha^2 \Phi \omega_\rho \omega^\rho - 3\square\Phi = 0, \quad (21)$$

where we have denoted $\Phi \equiv \phi^2$. The variation of the action (19) with respect to the scalar field ϕ is given by

$$R - 3\alpha \nabla_\rho \omega^\rho - \frac{3}{2} \alpha^2 \omega_\rho \omega^\rho - \Phi = 0, \quad (22)$$

This relation gives the equation of motion of the scalar field ϕ . From Eqs. (21) and (22) we find

$$\square\Phi - \alpha \nabla_\rho (\Phi \omega^\rho) = 0. \quad (23)$$

For the Weyl vector we obtain the equation of motion

$$4\xi^2 \nabla_\nu \tilde{W}^{\mu\nu} + \alpha^2 \Phi \omega^\mu - \alpha \nabla^\mu \Phi = 0. \quad (24)$$

The application to both sides of Eq. (24) of the operator ∇_μ leads to Eq. (23). Thus, the field equations of the theory are consistent.

3. Exact static analytical solution and the tangential rotation curves in Weyl geometric gravity

In the present Section we introduce an exact static, spherically symmetric solution of the field equations of the Weyl geometric gravity, obtained in a specific gauge in which the Weyl vector field has only a spacelike component [55, 56]. The expression of the tangential velocity of massive test particles moving in this geometry is also presented.

3.1. Exact solution of the Weyl geometric gravity field equations

In the following we will look for a static, spherically symmetric solution of the Weyl geometric gravity field equations. To this purpose we adopt a static and spherically symmetric geometry, and we introduce the set of coordinates (ct, r, θ, φ) on the base manifold. For the spacetime interval we adopt the expression [71]

$$ds^2 = e^{\nu(r)} c^2 dt^2 - e^{\lambda(r)} dr^2 - r^2 (d\theta^2 + \sin^2 \theta d\varphi^2), \quad (25)$$

where the metric coefficients are functions of the radial coordinate r only. We suppose that the Weyl vector ω_μ has only one non-vanishing component, and thus

$$\omega_\mu = (0, \omega_1(r), 0, 0). \quad (26)$$

For this form of ω_μ the Weyl field strength tensor vanishes identically, $\tilde{F}_{\mu\nu} \equiv 0$. Eq. (24) immediately gives

$$\Phi' = \alpha \omega_1 \Phi. \quad (27)$$

For the full set of the static spherically symmetric field equations of Weyl geometric gravity we refer the reader to Refs. [55, 56]. By assuming that the metric tensor components satisfy the condition $\nu + \lambda = 0$, the scalar field equation takes the form

$$\Phi'' - \frac{3}{2} \frac{\Phi'^2}{\Phi^2} = 0, \quad (28)$$

and it has the general solution

$$\Phi(r) = \frac{C_1}{C_2^2 \left(1 + \frac{r}{C_2}\right)^2}, \quad (29)$$

where C_1 and C_2 are arbitrary constants of integration. The radial component of the Weyl vector is given by

$$\omega_1(r) = \frac{1}{\alpha} \frac{\Phi'(r)}{\Phi(r)} = -\frac{2}{\alpha C_2} \frac{1}{1 + \frac{r}{C_2}}, \quad (30)$$

With the use of the above forms of the Weyl vector and of the scalar field, the field equations of the Weyl geometric gravity theory possess an exact solution, given by [55, 56],

$$\begin{aligned} e^{-\lambda(r)} &= e^{\nu(r)} = \frac{r(12C_3C_2^2 - C_1 - 4)}{4C_2} \\ &+ \frac{1}{4} (12C_3C_2^2 - C_1 - 8) \\ &+ \frac{C_2}{12} [12C_3C_2^2 - C_1 - 12] \frac{1}{r} + C_3 r^2, \end{aligned} \quad (31)$$

where C_3 is another arbitrary constant of integration.

The solution depends on three arbitrary independent integration. Depending on their parametrization, the exact solution (31) can be represented in several distinct ways forms. If we choose the constants so that they obey the condition, $12C_3C_2^2 - C_1 - 8 = 4$, or $C_3C_2^3 - C_1C_2/12 = C_2$, then the line element (31) becomes [55, 56]

$$e^{-\lambda(r)} = e^{\nu(r)} = 1 + \frac{2}{C_2}r + C_3r^2, \quad (32)$$

thus representing an extension of the de Sitter static, cosmological metric. From its form it follows that this metric is not asymptotically flat.

The parametrization of the metric (31) we will consider in the following is obtained by introducing a new variable r_g , according to the definition

$$\frac{C_2}{12} [12C_3C_2^2 - C_1 - 12] = -r_g. \quad (33)$$

We interpret $r_g = 2GM/c^2$ from a physical point of view as the gravitational radius of an object of mass M . Therefore, we obtain the following relations between the integration constants

$$12C_3C_2^2 - C_1 - 8 = 4(1 - 3r_g/C_2), \quad (34)$$

and

$$12C_3C_2^2 - C_1 - 4 = 4(2 - 3r_g/C_2), \quad (35)$$

respectively. For the integration constant C_3 we obtain the expression

$$C_3 = \frac{1}{C_2^2} \left(1 + \frac{C_1}{12} - \frac{r_g}{C_2} \right). \quad (36)$$

Therefore, with this parametrization of the integration constants, the metric (31) becomes

$$e^{\nu(r)} = e^{-\lambda(r)} = 1 - \frac{3r_g}{C_2} - \frac{r_g}{r} + \left(2 - 3\frac{r_g}{C_2} \right) \frac{r}{C_2} + \left(1 + \frac{C_1}{12} - \frac{r_g}{C_2} \right) \frac{r^2}{C_2^2}. \quad (37)$$

From Eq. (30) we obtain the constant C_2 as

$$C_2 = -\frac{\alpha}{2}\omega_1(r) - r. \quad (38)$$

From the expression of the scalar field (29) we find the relation

$$C_1 = \frac{4}{\alpha^2} \frac{\Phi(r)}{\omega_1^2}. \quad (39)$$

Note that a black hole solution similar to Eq. (37) was found in Weyl conformal gravity [31], and in the dRGT massive gravity theory [72].

3.2. Rotational velocities in static spherically symmetric geometries

The equations of motion of a massive particle in the gravitational field described by the general spherically symmetric metric (25) can be obtained from the Lagrangian [71, 73],

$$\mathcal{L}_W = \left[e^{\nu(r)} \left(\frac{cdt}{ds} \right)^2 - e^{\lambda(r)} \left(\frac{dr}{ds} \right)^2 - r^2 \left(\frac{d\Omega}{ds} \right)^2 \right], \quad (40)$$

By considering the motion restricted to the galactic plane with $\theta = \pi/2$ we obtain $d\Omega^2 = d\phi^2$. From the Lagrange equations it follows the existence of two constants of motion, the energy of the particle E , and its angular momentum l , respectively. Their expressions are given by $E = e^{\nu(r)}c^3\dot{t}$ and $l = cr^2\dot{\phi}$, respectively. Due to the normalization of the four-velocity as $u^\mu u_\mu = 1$, one can easily find the constraint $1 = e^{\nu(r)}c^2\dot{t}^2 - e^{\lambda(r)}\dot{r}^2 - r^2\dot{\phi}^2$, from which, with the use of the constants of motion, one finds the conserved energy of the particle as

$$\frac{E^2}{c^2} = e^{\nu+\lambda}\dot{r}^2 + e^\nu \left(1 + \frac{l^2}{c^2r^2} \right). \quad (41)$$

We interpret Eq. (41) as corresponding to the radial displacement of a massive particle in Newtonian mechanics. The particle has a velocity \dot{r} , a position dependent effective mass $m_{\text{eff}}(r) = 2e^{\nu(r)+\lambda(r)}$, and, of course, a conserved energy E^2 . The motion takes place in the presence of an effective potential $V_{\text{eff}}(r)$, which can be obtained as

$$V_{\text{eff}}(r) = e^{\nu(r)} \left(1 + \frac{l^2}{c^2r^2} \right). \quad (42)$$

For stable circular particle orbits, satisfying the conditions $\dot{r} = 0$ and $\partial V_{\text{eff}}/\partial r = 0$, respectively, the conserved energy and angular momentum become

$$\frac{E^2}{c^4} = \frac{e^\nu}{1 - r\nu'/2}, \quad \ell^2 = \frac{c^2}{2} \frac{r^3\nu'}{1 - r\nu'/2}, \quad (43)$$

The spatial velocity v of the massive particle is obtained as [71]

$$v^2(r) = e^{-\nu} \left[e^\lambda \left(\frac{dr}{dt} \right)^2 + r^2 \left(\frac{d\Omega}{dt} \right)^2 \right]. \quad (44)$$

For $\dot{r} = 0$ the tangential velocity of a massive test particles has the expression

$$v_{\text{ig}}^2(r) = e^{-\nu}r^2 \left(\frac{d\Omega}{dt} \right)^2 = e^{-\nu}r^2c^2 \left(\frac{d\Omega}{ds} \right)^2 \left(\frac{ds}{cdt} \right)^2. \quad (45)$$

For a motion in the equatorial plane with $\theta = \pi/2$, we find for the tangential velocity the simple expressions

$$\frac{v_{\text{ig}}^2(r)}{c^2} = c^2 \frac{e^\nu}{r^2} \frac{\ell^2}{E^2}, \quad (46)$$

and

$$\frac{v_{\text{ig}}^2(r)}{c^2} = \frac{r\nu'}{2}, \quad (47)$$

respectively.

By using the above expression of the tangential velocity, the angular momentum of the particle can be written as

$$\ell^2 = r^2 \frac{v_{tg}^2(r)}{1 - v_{tg}^2(r)/c^2}. \quad (48)$$

For the effective potential we obtain

$$V_{eff}(r) = \frac{e^{v(r)}}{1 - v_{tg}^2(r)/c^2}. \quad (49)$$

If the tangential velocity of massive test particles can be found from observational data, or by using some theoretical models, one can obtain the metric tensor component $v(r)$ in the dark matter dominated region of a galaxy as

$$v(r) = 2 \int \frac{v_{tg}^2(r) dr}{c^2 r}. \quad (50)$$

3.3. Tangential velocity in Weyl geometric gravity

In the case of the static spherically symmetric exact solution of Weyl geometric gravity, with line element given by Eq. (37) we have

$$v' = \frac{\frac{r_g}{r^2} + \left(2 - 3\frac{r_g}{C_2}\right)\frac{1}{C_2} + 2\left(1 + \frac{C_1}{12} - \frac{r_g}{C_2}\right)\frac{r}{C_2^2}}{1 - \frac{3r_g}{C_2} - \frac{r_g}{r} + \left(2 - 3\frac{r_g}{C_2}\right)\frac{r}{C_2} + \left(1 + \frac{C_1}{12} - \frac{r_g}{C_2}\right)\frac{r^2}{C_2^2}}, \quad (51)$$

giving for the tangential velocity the expression

$$\frac{2v_{tg}^2}{c^2} = \frac{\frac{r_g}{r} + \left(2 - 3\frac{r_g}{C_2}\right)\frac{r}{C_2} + 2\left(1 + \frac{C_1}{12} - \frac{r_g}{C_2}\right)\frac{r^2}{C_2^2}}{1 - \frac{3r_g}{C_2} - \frac{r_g}{r} + \left(2 - 3\frac{r_g}{C_2}\right)\frac{r}{C_2} + \left(1 + \frac{C_1}{12} - \frac{r_g}{C_2}\right)\frac{r^2}{C_2^2}}, \quad (52)$$

or,

$$v_{tg} = c \sqrt{2r} \sqrt{\frac{1 + 2\left(1 - \frac{3}{2}\frac{r_g}{C_2}\right)\frac{r^2}{r_g C_2} + 2\left(1 + \frac{C_1}{12} - \frac{r_g}{C_2}\right)\frac{r^3}{r_g C_2^2}}{1 - \frac{3r_g}{C_2} - \frac{r_g}{r} + 2\left(1 - \frac{3}{2}\frac{r_g}{C_2}\right)\frac{r}{C_2} + \left(1 + \frac{C_1}{12} - \frac{r_g}{C_2}\right)\frac{r^2}{C_2^2}}}. \quad (53)$$

The first term in the above equation is nothing but the Keplerian velocity of the particle, $v_K = \sqrt{GM/r}$. The second term gives the Weyl geometrical corrections to the ordinary Newtonian velocity.

In the following we assume that M represents the baryonic mass of the galaxy. For a baryonic mass of the order of $M = 10^{10} M_\odot$, $r_g = 2GM/c^2$ has the value $r_g = 2.96 \times 10^{15}$ cm. Taking into account that $1 \text{ kpc} = 3.08 \times 10^{21}$ cm, and that $1 \text{ cm} = 1/3.08 \times 10^{21} \text{ kpc}$, it follows that $r_g = 9.61 \times 10^{-7} \approx 10^{-6}$ kpc. However, one can assume for r_g a range of $r_g \in (10^{-8}, 10^{-4})$ kpc.

The constant C_2 has the physical dimensions of length, and it can take both positive and negative values. If $C_2 > 0$, it must satisfy the condition $C_2 \gg 3r_g$, so that the term $1 - 3r_g/C_2$ in the metric is always positive, and tends to 1 in the Newtonian limit. There are no similar restrictions for negative values of C_2 . C_2 is related to the behavior of the Weyl vector field.

On the other hand, C_1 is a dimensionless constant, describing the magnitude of the auxiliary scalar field. Similarly to C_2 , it can take both positive and negative numerical values. In order to avoid any singular or unphysical behavior in the metric for small r , we assume that the range of the radial coordinates is restricted to values $r > r_g$.

In the limit $|C_2| \rightarrow \infty$, we reobtain from Eq. (53) the general relativistic limit of the tangential velocity,

$$\lim_{|C_2| \rightarrow \infty} v_{tg} = c \sqrt{\frac{r_g}{2r} \left(1 - \frac{r_g}{r}\right)^{-1/2}}, \quad (54)$$

corresponding to the Schwarzschild metric with $e^v = 1 - r_g/r$. In the limiting case $r \rightarrow \infty$, we have $v_{tg} \rightarrow c$, that is, the velocity of the test particles tend to the speed of light. However, if the integration constants satisfy the condition $1 + C_1/12 - r_g/C_2 = 0$, in the large r limit the tangential velocity tends to $\lim_{r \rightarrow \infty} v_{tg} = c/\sqrt{2}$.

For large values of r , the tangential velocity behaves as

$$\begin{aligned} \frac{v_{tg}^2}{c^2} &\approx 1 + \frac{6C_2(3r_g - 2C_2)}{r[(C_1 + 12)C_2 - 12r_g]} \\ &+ \frac{12C_2^2[-(C_1 - 12)C_2^2 + 3(C_1 - 8)C_2r_g + 18r_g^2]}{r^2[(C_1 + 12)C_2 - 12r_g]^2} \\ &+ O\left(\left(\frac{1}{r}\right)^3\right), \end{aligned} \quad (55)$$

which also show that in the limit of large r the tangential velocity tends towards the speed of light.

4. Fitting the Weyl geometric rotation curves with the SPARC sample

In the present Section we consider a detailed comparison of the theoretical predictions of the tangential velocities obtained from the exact solution of Weyl geometric gravity with the observational data. For this comparison we use the data of the SPARC sample, which contains the rotation curves of a large number of galaxies,

We consider galaxies both with and without bulge velocities, and we perform the comparison with all galaxies having an acceptable number of observational points.

4.1. The SPARC dataset

The SPARC sample consists of the rotation curves data of 175 galaxies [59–61]. In the sample all rotationally supported morphological galactic types are included. The distribution of the galaxies of the SPARC sample according to their morphological types are presented in Fig. 1. As one can see from Fig. 1), the SPARC sample contains data on a large variety of galaxy types.

A large number of astrophysical/astronomical data are also provided in the SPARC sample, including the Hubble types, distance, inclination, total luminosity, effective radius, and effective surface brightness at [3.6], total HI mass, and the asymptotically flat rotation velocity, respectively.

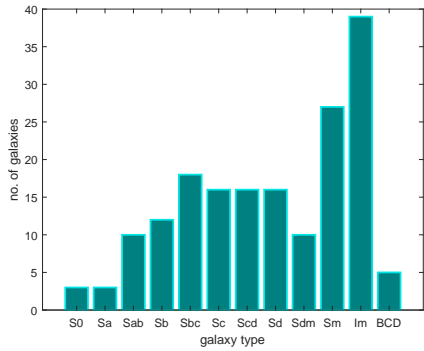


Figure 1: Distribution of the galaxies of the SPARC sample according to their morphological type.

The distance and radius distributions of the galaxies in the sample are shown in Fig. 2.

Data on the distribution of the stellar masses, together with 21 cm observations, tracing the atomic gas, are also added to the sample. The rotation curves are obtained from the 21 cm velocity fields [59–61], and information on the observations of the ionized interstellar medium are also provided.

Up to now, the SPARC sample is the largest existing galactic database, giving for every galaxy not only the rotation curves, but also spatially resolved data, showing the distribution of both stars and gas [59–61].

The SPARC sample contains galaxies with rotation velocities in the range $20 < V_f < 300$ km/s, and luminosities in the interval $10^7 < L_{[3.6]} < 5 \times 10^{11} L_\odot$. The distribution of the galactic luminosities and of the Asymptotically Flat Rotation Velocities of the galaxies in the SPARC dataset is presented in Fig. 3.

The distribution of the number of data points for the observations of the galactic rotation curves, as well as their quality flags, are presented in Fig. 4.

The SPARC dataset contains significant information not only about large individual galaxies, but as well as about small ones. Moreover, low surface brightness and low mass galaxies are also well represented in SPARC [59–61]. This represents a significant difference as compared to flux selected samples, which contain data only on the interval $M_* > 10^9 M_\odot$, and $V_f > 100$ km/s, respectively [61].

4.2. Material and methods

To test the validity of the expression of the velocity of the test particles in the Weyl geometric gravity theory, as given by Eq. (53), we have fitted the predicted theoretical velocity profile with the total observational velocity of the particles that can be obtained from the SPARC database. In the following we will present first the theoretical model used for obtaining the fits.

4.2.1. The theoretical model

We assume that the total velocity v_t can be obtained from the relation [61]

$$v_t = \sqrt{v_g |v_g| + \Upsilon_d \times v_d |v_d| + \Upsilon_b \times v_b |v_b| + v_{tg}^2}, \quad (56)$$

where v_t is the total velocity, including the contributions of both baryonic and dark matter, and v_g , v_d , v_b and v_{tg} denote the contributions from the velocity of the gas, of the disk, of the bulge, and of the Weyl geometric gravity effects, respectively. Υ_d and Υ_b denote the stellar mass-to-light ratios for the disk and the stellar bulge, respectively.

4.2.2. The fitting procedure

To perform the fitting, and by taking into account the observational errors, we have looked for the minimum of the objective function

$$\chi^2(r_g, C_1, C_2, \Upsilon_d, \Upsilon_b) = \frac{1}{n-k} \sum_{i=1}^n \frac{(v_{t,i} - v_{obs,i})^2}{\sigma_i^2}, \quad (57)$$

where n is the length of data, and k is the number of parameters that must be estimated, that is, $k = 4$ for bulgeless galaxies, and $k = 5$ for galaxies with bulge velocity data, respectively. We selected the galaxies with length data larger than the number of parameters to be optimized (4, respectively 5). We used Multi Start and Global Search methods (see [74] for a full description of the algorithm and the scatter-search method of generating trial points). For both methods the solver attempts to find multiple local solutions to an optimization problem by starting from various points. Global Search analyzes start points, discarding ones that are improbable to improve the current best local minimum. On the other hand, Multi Start runs the local solver on all start points (or, optionally, all those that meet feasibility criteria concerning bounds or inequality constraints.). In the present investigation the number of start points was set to 10000.

The intervals for the parameters appearing in the tangential velocity were chosen as follows: $r_g \in [10^{-23}, 10^{-2}]$, $C_1 \in [-10^{11}, 10^{14}]$, $C_2 \in [-10^{11}, 10^{14}]$. We also imposed the condition $r_g/C_2 < 1$, and we have limited the values of Υ_d and Υ_b to the interval [0.1,5].

4.3. Fitting results

In the following we consider independently the two group of galaxies without and with bulge velocity information. The number of fitting parameters is different in the two cases (4 respective 5).

4.4. Fitting results for galaxies without bulge velocity information

As a first example of the comparison of the theoretical model of the rotation curves as given by Weyl geometric gravity and observations we consider the fitting of the galaxies of the SPARC sample that do not have a bulge velocity component. The number of galaxies we have considered in our analysis is 76. The comparison of the observational data and of the theoretical model are presented, for a selected sample of 55 galaxies, in Figs. 6, 7, and 8, respectively.

In each plot we have presented, for each galaxy, the observational data with their error bars, the contribution of the baryonic matter, the contribution coming from the Weyl geometric gravity, as well as the total velocity, as given by Eq. (56).

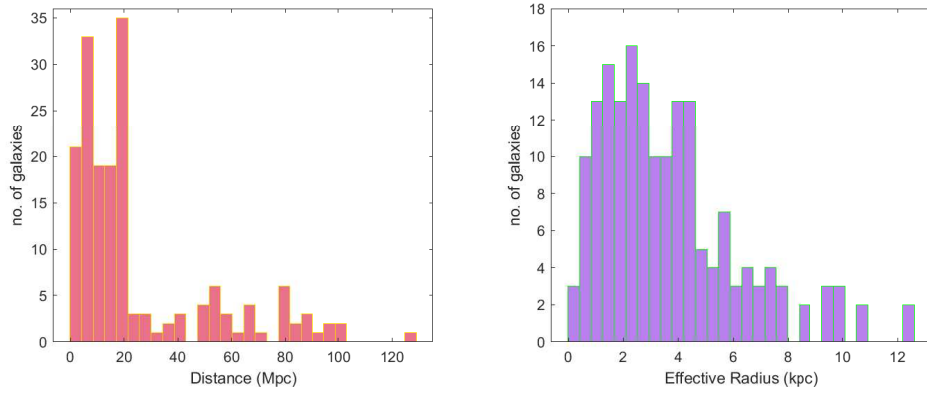


Figure 2: Distribution of the galactic distances (left panel) and of the effective radius (right panel) in the SPARC sample.

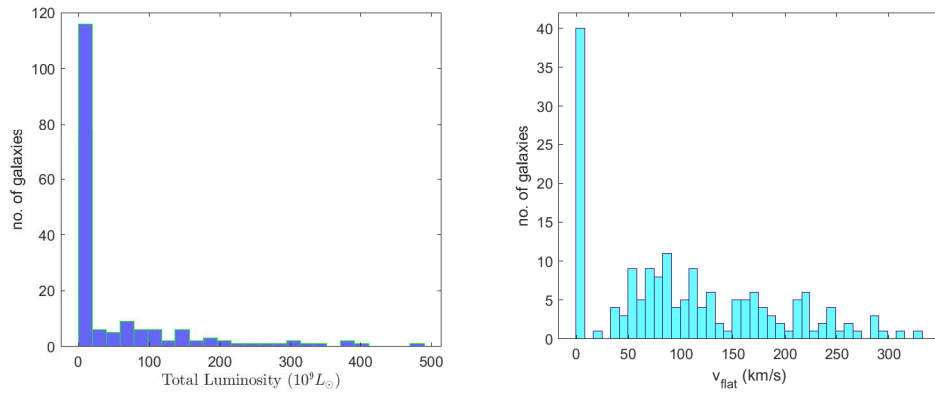


Figure 3: Distribution of the galactic luminosities (left panel) and of the Asymptotically Flat Rotation Velocities of the galaxies (right panel) in the SPARC dataset.

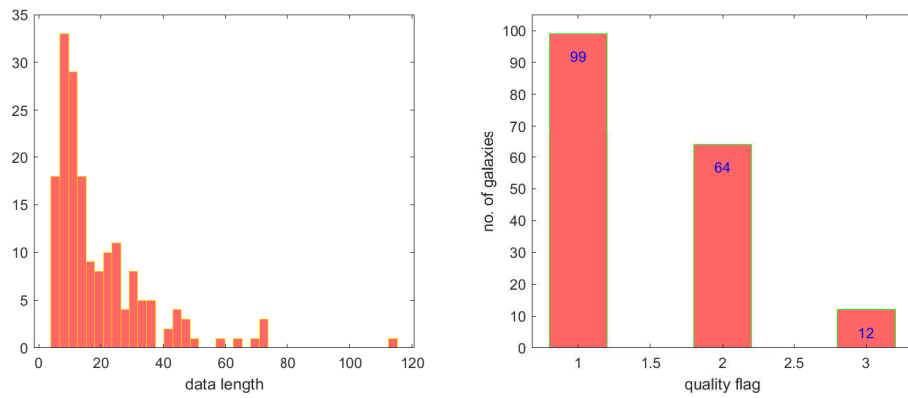


Figure 4: Distribution of the number of the observational points (left panel) and of the quality flag (right panel) in the SPARC sample.

The numerical values of the model parameters (r_g, C_1, C_2) , obtained from the fitting, are presented, for this set of 55 galaxies, in Tables 1, 2, and 3, respectively. As one can see from the Tables, for this set of 55 SPARC galaxies, all the values of χ^2 are smaller than 1, indicating a good fit of the theoretical model with the observational data.

With respect to the model parameters, one observes first the very small values of r_g for all galaxies. r_g encodes the baryonic matter contribution coming from the Schwarzschild type component of the metric. On the other hand, the baryonic matter component is also contained in the observational data for $v_{bar} = \sqrt{v_g|v_g| + \Upsilon_d \times v_d|v_d| + \Upsilon_b \times v_b|v_b|}$ indicating that the possible contribution of baryonic matter from the Weyl metric is negligibly small.

In the present parameterizations, and investigations of the Weyl metric we do not assume that the term proportional to r^2 is of purely cosmological origin, and hence we do not identify the coefficient $1 + C_1/12 - r_g/C_2$ with the cosmological constant Λ . We consider this term as intrinsically belonging to the mathematical structure of the metric, and giving physical effects independent of the cosmological background.

Hence, C_1 and C_2 are independent quantities, describing the properties of the Weyl vector, and of the scalar field, which are determined by the local astrophysical properties of the galaxies. Thus, their range and magnitude of values are strictly galaxy-dependent. The constant C_1 takes generally negative values, with the exception of a few galaxies. C_1 is a dimensionless parameter, taking values in the range $10^7 - 10^8$. Its mean value for the considered set of bulgeless galaxies is $\langle C_1 \rangle = 4.097 \times 10^9$.

From a physical point of view, as one can see from Eq. (29), C_1 describes the distribution of the numerical values of the auxiliary scalar field $\Phi(r)$, which is related, via Eqs. (14) and (22) to the Weyl curvature scalar as $\tilde{R} = \Phi$. This allows to obtain the behavior of \tilde{R} in the dark matter halo of the galaxies, and directly reconstruct the Weyl geometric features of the galactic spacetime. The variations of the scalar field Φ and of the Weyl vector component $\alpha\omega_1$ inside a small selected sample of galaxies are presented in Fig. 5.

The constant C_2 is a dimensional constant, having dimensions of length. The fitting of the galactic rotation curves gives for C_2 values of the same order of magnitude as for C_1 , $C_2 \in \{10^7, 10^8\}$ kpc, which are much larger values as compared to the extension of the galactic dark matter halo, having values of the order of a few tenths of kiloparsecs. The mean value of the constant C_2 is obtained, for the considered set of bulgeless galaxies, as $\langle C_2 \rangle = 3.3478 \times 10^8$ kpc.

Since $r \ll C_2$, one can estimate the magnitude of scalar field as being given by $\Phi \approx C_1/C_2^2$, while for the Weyl vector we obtain $\omega_1 \approx -2/\alpha C_2$. For the approximate average values of the scalar field we obtain $\langle \Phi \rangle = \langle C_1/C_2^2 \rangle = 1.04 \times 10^{-8}$ kpc $^{-2}$, and $\langle \Phi \rangle = \langle C_1 \rangle / \langle C_2 \rangle^2 = 3.65 \times 10^{-8}$ kpc $^{-2}$. In the case of the Weyl vector there is an extra-dependence on the Weyl coupling constant α .

Finally, the mass to light ratios Υ_d have relatively small values for all galaxies, exceeding the value one in very few cases.

This indicates the realistic nature of the fits, which do not require the introduction of unphysical parameters characterizing baryonic matter.

4.5. Correlations of the optimal parameters

In order to check the correlation of the optimal parameters found for each galaxy we made the analysis of the objective function χ^2 . We took all pairs of two values from the four (respectively five parameters) and we constructed grids of 100X100 points around these optimal values and then we computed the values of χ^2 on these grids keeping the other parameters equal to their optimal values.

We plotted the isolines of the values of χ^2 for four galaxies without bulge velocity data in Figs. 9, and 10, respectively. Hence, the isolines show the pairs of parameters for which we obtain the same value of χ^2 .

We observe that an increase of r_g corresponds to a decrease of C_1 (showing that they are anticorrelated), an increase of C_2 (so r_g and C_2 are correlated), and a decrease of Υ_d and Υ_b (so r_g is anti-correlated with Υ_d and Υ_b) etc.

Finally, if we increase the value of Υ_d we obtain the same values of χ^2 as for the smaller values of Υ_b (which is to be expected because if the contribution of the disk to the total velocity increases, the contribution of the bulge must decrease and viceversa).

4.6. Fitting of the galaxies with bulge velocity data

The results of the fitting of a sample of 20 galaxies with bulge velocities are presented in Fig. 11. The optimal values of the model parameters, and of the mass to light ratios are presented, together with the χ^2 values, in Table 4. Similarly to the bulgeless case, the parameter r_g takes very small values, indicating that the baryonic matter component, as obtained from the corresponding baryonic velocity distribution, is enough for the interpretation of the data, and no extra baryonic component is needed.

The numerical values of the constants C_1 and C_2 are in the same quantitative range as in the bulgeless case. The constant C_1 takes again negative values, while C_2 is always positive, and takes large values, exceeding those taken by the radial coordinate inside the galactic halo. The mean value of the constant C_1 for the galaxies with bulge velocity contribution is $\langle C_1 \rangle = 2.01 \times 10^7$, while the mean value of the constant C_2 is $\langle C_2 \rangle = 5.79 \times 10^7$ kpc $^{-2}$. For the mean values of the scalar field we obtain $\langle \Phi \rangle = \langle C_1/C_2^2 \rangle = 9.08 \times 10^{-9}$ kpc $^{-2}$, and $\langle \Phi \rangle = \langle C_1 \rangle / \langle C_2 \rangle^2 = 5.99 \times 10^{-9}$ kpc $^{-2}$, respectively.

The two mass to light ratios have acceptable values, and only in a few cases values of Υ_d bigger than one are necessary for the fitting. The distribution of the χ^2 function indicates a values ranging from $\chi^2 = 0.022$ to $\chi^2 = 2.046$, with most of values in the range $\chi^2 < 1$. These results show that the Weyl geometric gravity model can provide acceptable fits for the observational data even for this set of observations.

The isolines of the χ^2 distribution for a small set of galaxies with bulge velocity are presented in Figs. 12, and 13, respectively.

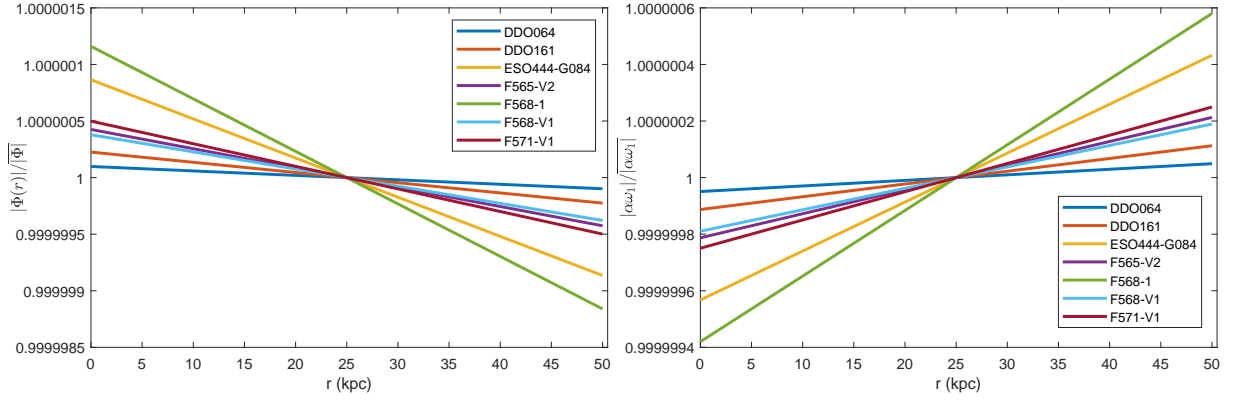


Figure 5: Variation of the scalar field $|\Phi|$ and of $|\alpha\omega_1|$ inside a selected sample of SPARC galaxies.

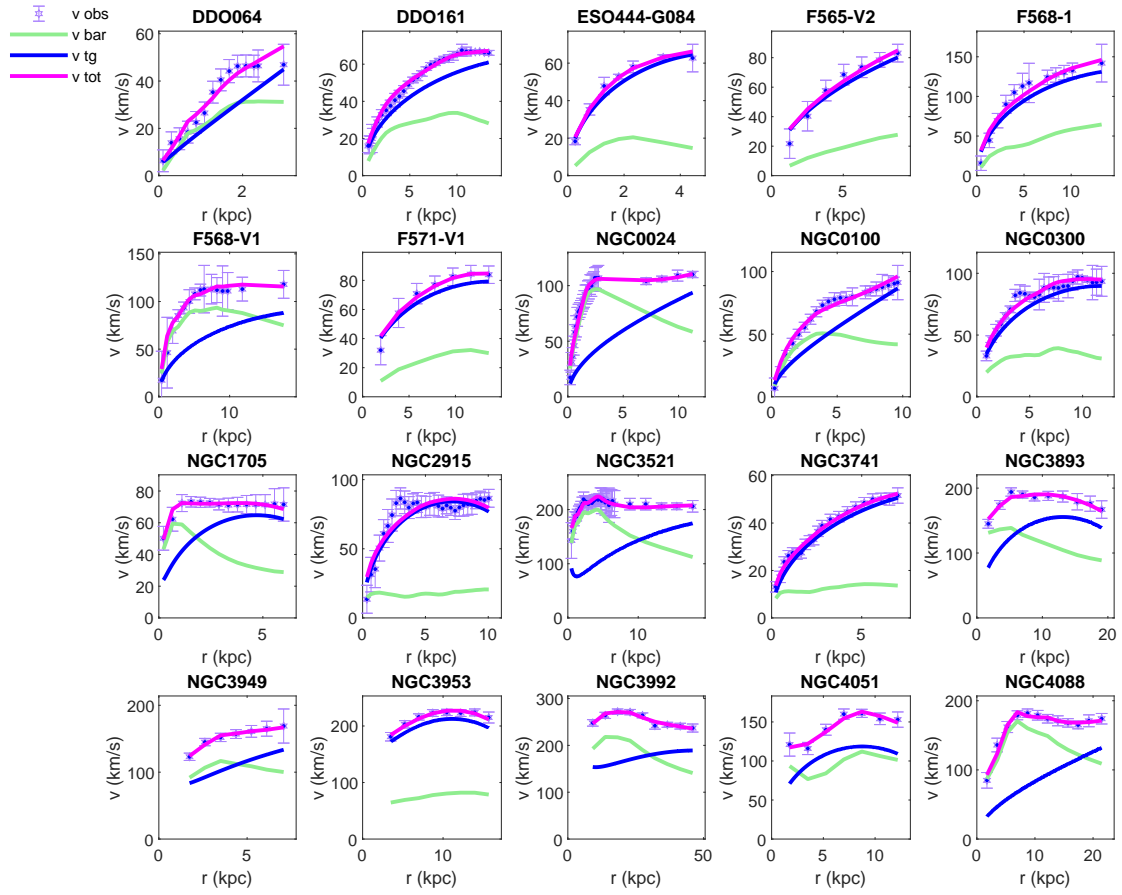


Figure 6: Rotation velocities for 20 SPARC galaxies without bulge velocity information data.

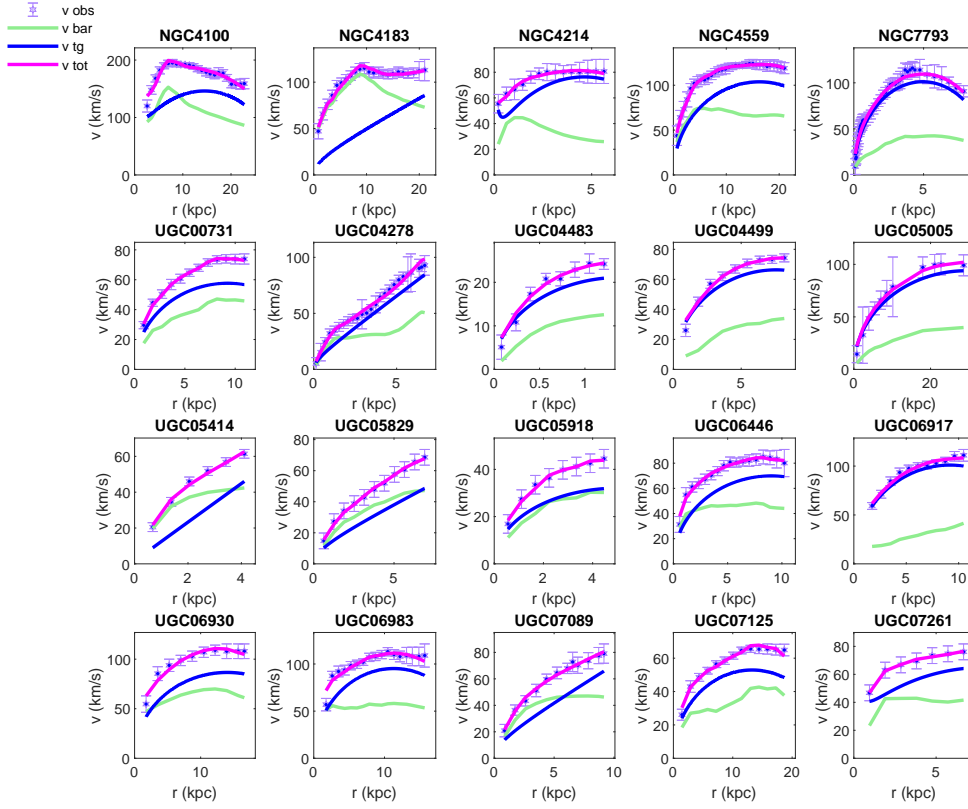


Figure 7: Rotation velocities for 20 SPARC galaxies without bulge velocity data.

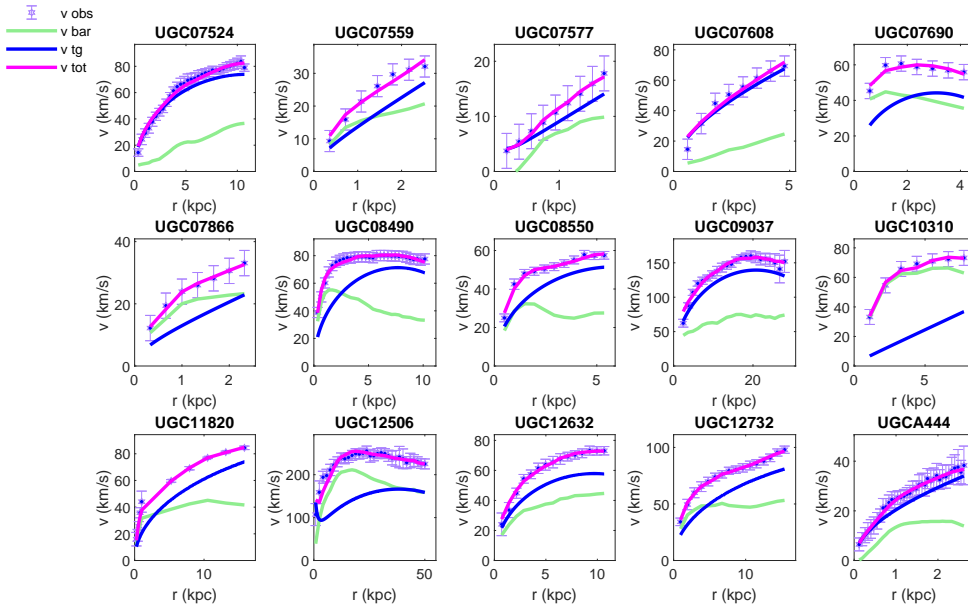


Figure 8: Rotation velocities for 15 SPARC galaxies without bulge velocity data.

Galaxy	r_g (kpc)	C_1	C_2 (kpc)	Υ_d (M_\odot/L_\odot)	χ^2
DDO064	3.787e-11	5788848096.401	508041269.342	1.622	0.507
DDO161	1.000e-23	-62562119.155	221736484.801	0.100	0.572
ESO444-G084	1.000e-23	-61854532.467	57806524.365	0.100	0.754
F565-V2	1.000e-23	-7088925.839	117472239.881	0.100	0.618
F568-1	1.000e-23	-14758985.776	43093995.313	0.770	0.988
F568-V1	1.000e-23	-31757405.870	131985481.647	3.945	0.163
F571-V1	1.000e-23	-42902459.034	100172907.865	0.100	0.379
NGC0024	1.000e-23	26031816.009	135988296.772	1.865	0.348
NGC0100	1.000e-23	206024986.877	207322173.434	0.800	0.821
NGC0300	1.000e-23	-33489958.963	65784650.850	0.394	0.644
NGC1705	9.366e-10	-64483678.485	50613780.152	1.664	0.121
NGC2915	1.000e-23	-38060413.192	45210549.727	0.100	0.915
NGC3521	8.146e-08	-7292886.158	37530429.456	0.499	0.169
NGC3741	1.000e-23	-86254273.703	175001374.119	0.462	0.366
NGC3893	1.000e-23	-11155699.476	24390676.761	0.413	0.594
NGC3949	8.391e-08	-7906447.099	31235899.217	0.327	0.273
NGC3953	5.859e-07	-6296420.542	12002585.314	0.100	0.396
NGC3992	2.526e-06	-8063470.748	66178422.212	0.781	0.526
NGC4051	1.000e-23	-19177151.045	28032452.130	0.306	0.692
NGC4088	1.000e-23	32561648.876	152931196.546	0.402	0.494

Table 1: Optimal values of the parameters for the galaxies whose rotation velocities are plotted in Fig 6.

Galaxy	r_g (kpc)	C_1	C_2 (kpc)	Υ_d (M_\odot/L_\odot)	χ^2
NGC4100	2.083e-07	-13013217.619	31954992.408	0.534	0.650
NGC4183	1.000e-23	452475377.873	597226941.898	1.637	0.246
NGC4214	9.673e-09	-47027873.229	36541360.348	0.524	0.076
NGC4559	1.000e-23	-25031486.089	67875858.531	0.385	0.098
NGC7793	1.000e-23	-26348417.531	21709425.077	0.100	0.576
UGC00731	1.000e-23	-81127914.722	125161386.432	5.000	0.101
UGC04278	1.000e-23	2200684669.177	366439884.486	0.923	0.454
UGC04483	1.000e-23	-603007109.979	141169326.943	0.100	0.771
UGC04499	1.000e-23	-61295667.386	77406914.217	0.100	0.699
UGC05005	1.000e-23	-30551927.021	149493907.016	0.100	0.177
UGC05414	1.000e-23	80431750353.603	2280981528.847	1.061	0.778
UGC05829	1.000e-23	1349304293.380	602130434.197	2.522	0.053
UGC05918	1.000e-23	-262450081.090	220573114.601	2.327	0.128
UGC06446	1.000e-23	-55187096.744	82990617.223	1.811	0.195
UGC06917	1.000e-23	-26428443.948	40479816.606	0.100	0.535
UGC06930	1.000e-23	-35940098.272	84004991.006	0.799	0.501
UGC06983	1.000e-23	-29767444.028	56137365.807	0.782	0.629
UGC07089	1.000e-23	851698942.747	458950441.378	0.697	0.157
UGC07125	1.000e-23	-96323598.406	212796623.635	0.340	0.601
UGC07261	1.564e-08	-65132116.799	87859036.829	0.688	0.028

Table 2: Optimal values of the parameters for the galaxies whose rotation velocities are plotted in Fig 7.

Galaxy	r_g (kpc)	C_1	C_2 (kpc)	Υ_d (M_\odot/L_\odot)	χ^2
UGC07524	1.000e-23	-49350136.845	90321980.010	0.100	0.517
UGC07559	1.000e-23	5370120200.786	764005723.368	0.658	0.515
UGC07577	4.381e-11	66656987997.450	3104152296.378	0.100	0.030
UGC07608	1.000e-23	51193449.496	111393221.187	0.100	0.581
UGC07690	1.000e-23	-137870331.963	71148385.044	0.784	0.506
UGC07866	1.000e-23	3077280935.014	724351653.383	1.258	0.047
UGC08490	1.000e-23	-53025454.948	67806785.219	1.350	0.212
UGC08550	1.000e-23	-101438913.618	99962034.196	1.126	0.508
UGC09037	1.000e-23	-13869977.750	48003507.625	0.100	0.939
UGC10310	1.000e-23	56281824440.461	4578269948.117	2.396	0.189
UGC11820	1.000e-23	-28209554.429	214936509.292	1.663	0.460
UGC12506	3.149e-07	-9874154.696	63305217.998	1.370	0.554
UGC12632	1.000e-23	-80421187.018	130076378.298	1.413	0.220
UGC12732	1.000e-23	-27533667.612	166645457.180	1.827	0.131
UGCA444	1.000e-23	103957781.561	223885591.848	0.100	0.056

Table 3: Optimal values of the parameters for the galaxies whose rotation velocities are plotted in Fig 8.

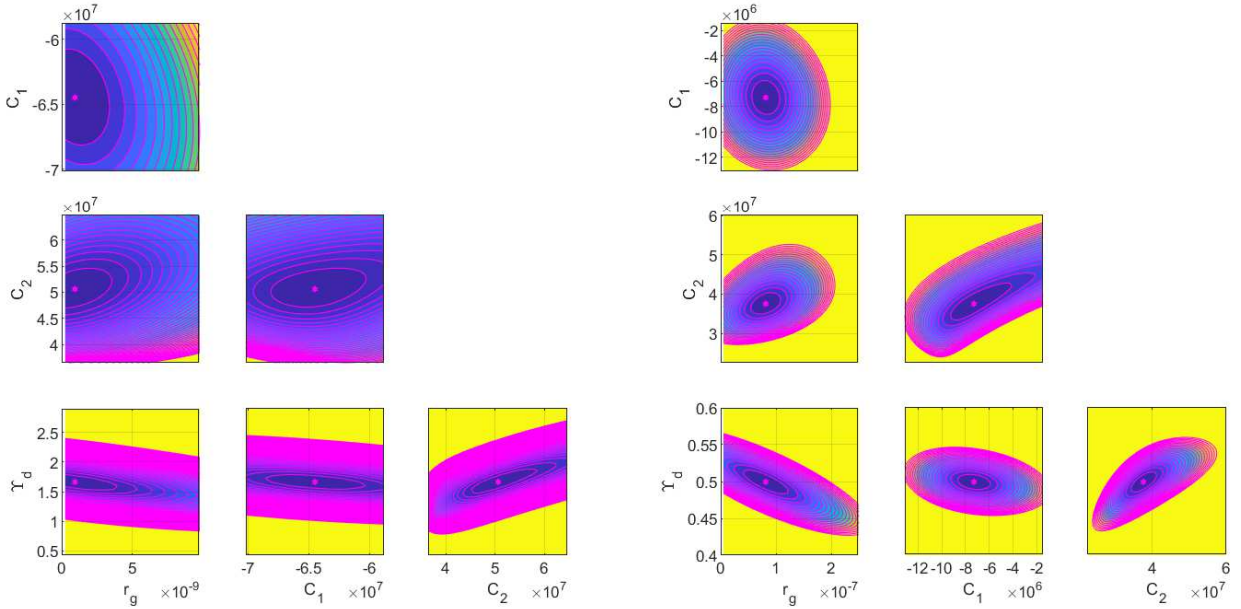


Figure 9: Isolines of the χ^2 surfaces around optimal parameters for the galaxy NGC1705 (left panel), and for the galaxy NGC3521 (right panel).

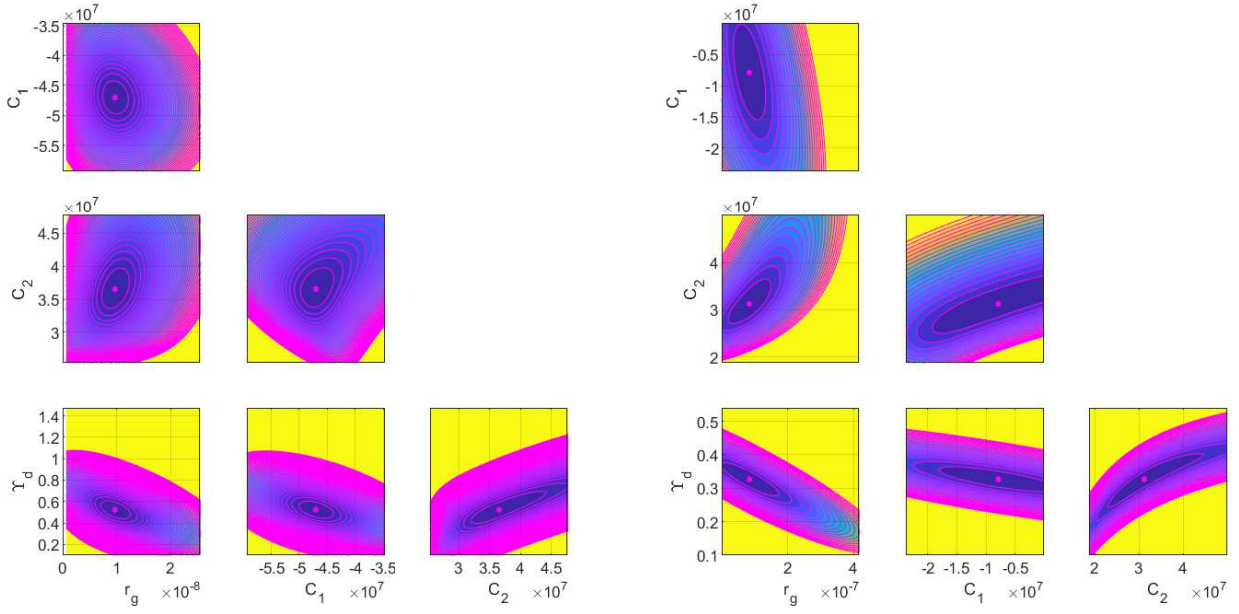


Figure 10: Isolines of the χ^2 surfaces around optimal parameters for the galaxy NGC4214.

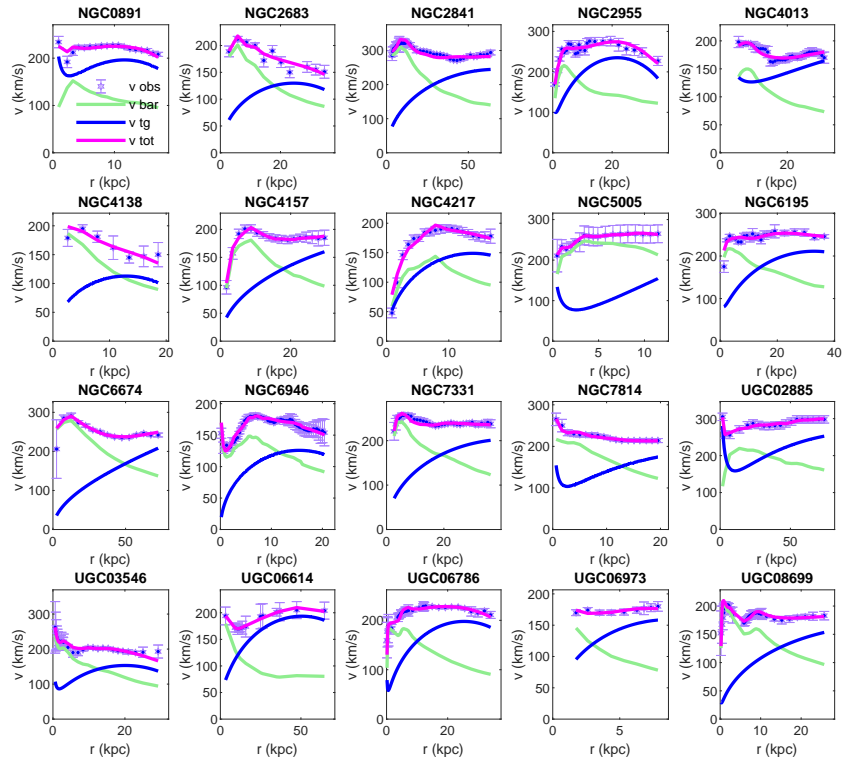


Figure 11: Rotation velocities for 20 galaxies with bulge velocity data.

Galaxy	r_g (kpc)	C_1	C_2 (kpc)	Υ_d (M_\odot/L_\odot)	Υ_b (M_\odot/L_\odot)	χ^2
NGC0891	7.406e-07	-7548219.795	15253073.451	0.197	0.100	1.234
NGC2683	1.000e-23	-16000065.073	65051713.809	0.753	0.100	1.604
NGC2841	1.080e-13	-4496210.516	50623362.039	1.246	0.884	1.748
NGC2955	1.102e-07	-4902267.287	17830128.465	0.100	0.674	1.687
NGC4013	1.616e-06	-5131504.307	97579798.795	0.494	0.100	0.743
NGC4138	1.000e-23	-21176828.022	45559450.954	0.855	0.100	2.046
NGC4157	1.001e-23	-5894284.347	86512981.587	0.503	0.100	0.265
NGC4217	1.000e-23	-12151305.398	28073861.051	1.181	0.123	1.854
NGC5005	1.913e-07	232753862.401	124443725.256	0.614	0.365	0.022
NGC6195	8.931e-08	-6061759.524	33240834.431	0.100	0.687	1.647
NGC6674	4.387e-11	5395586.701	177645686.226	1.248	1.598	1.341
NGC6946	1.000e-23	-17033560.155	43947101.122	0.475	0.519	1.507
NGC7331	1.001e-23	-6500574.938	47160989.502	0.421	0.100	0.845
NGC7814	3.157e-07	-7302964.454	42596044.256	1.749	0.372	0.408
UGC02885	2.890e-06	-3936362.944	70070401.820	0.778	0.100	0.173
UGC03546	1.407e-07	-11648346.858	39256891.791	0.595	0.351	0.888
UGC06614	5.654e-08	-7209010.216	60761899.115	0.100	0.521	0.023
UGC06786	2.048e-08	-6897154.187	29136907.700	0.766	0.752	1.609
UGC06973	1.001e-23	-10669113.237	15495630.244	0.177	0.100	0.751
UGC08699	2.852e-09	-9693947.277	68352653.068	1.029	0.605	0.665

Table 4: Optimal values of the parameters for the galaxies with bulge whose rotation velocities are plotted in Fig 11.

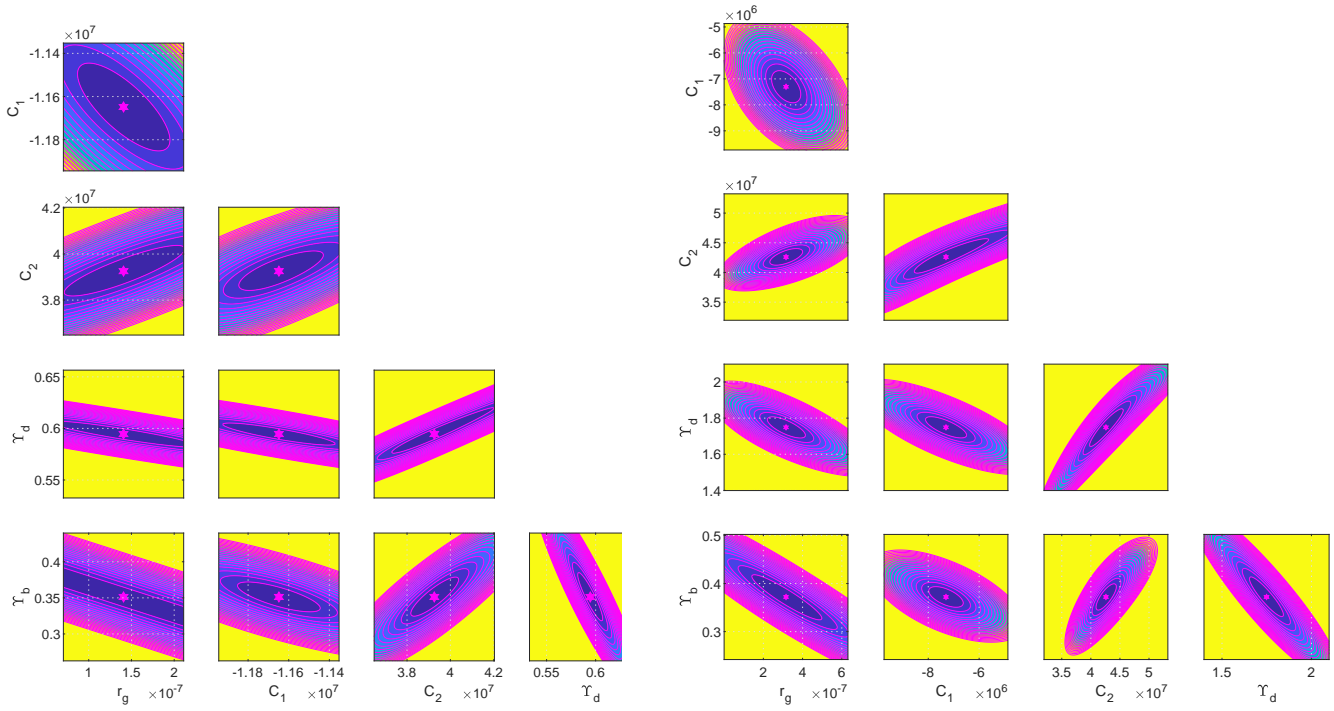


Figure 12: Isolines of the χ^2 surfaces around optimal parameters for the galaxy UGC03546 (left panel) and for the galaxy NGC7814 (right panel).

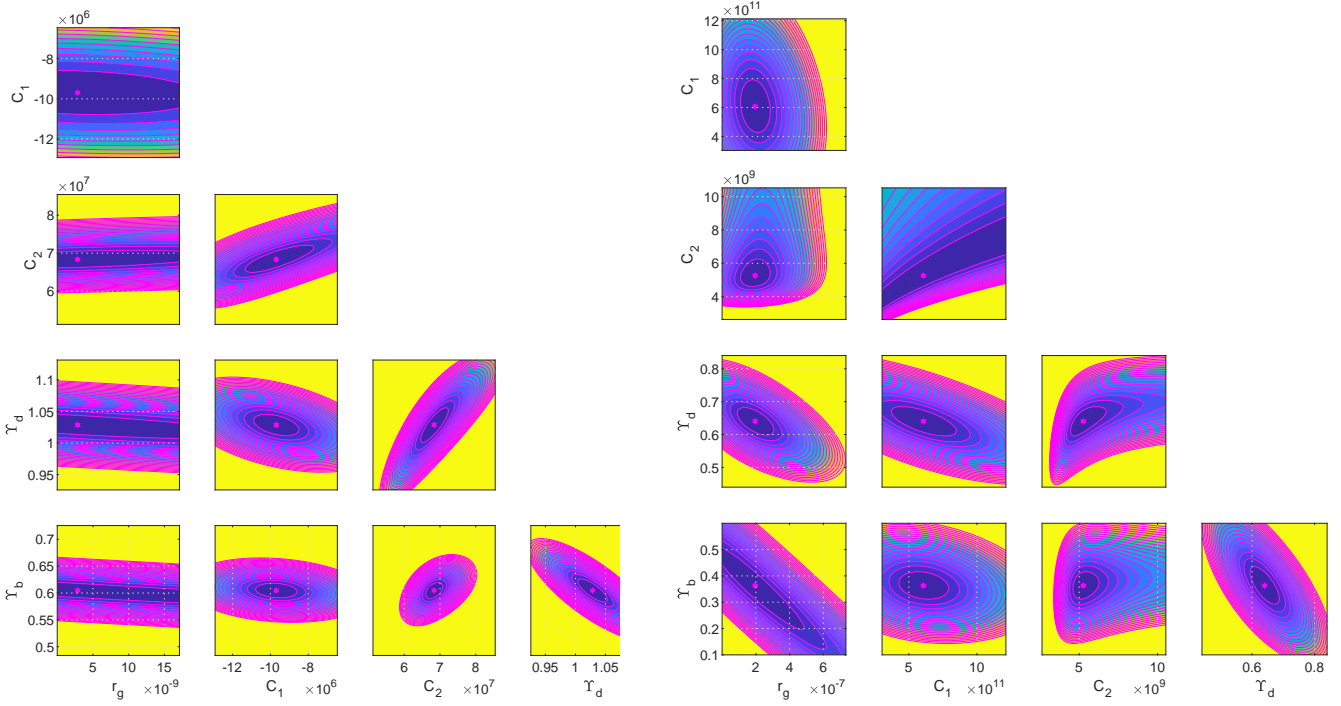


Figure 13: Isolines of the χ^2 surfaces around optimal parameters for the galaxy UGC08699 and for the galaxy NGC5005.

4.7. Optimal parameters distribution

In the following we consider the distributions of the various statistical parameters of the Weyl geometric gravity dark matter model.

χ^2 distribution of the SPARC sample.. Fig. 14 presents the distribution of the values of the objective function χ^2 for the total number of the considered galaxies for which $\chi^2 \leq 10$. One can observe that there are 86 galaxies with $\chi^2 < 1$, 37 galaxies with χ^2 between 1 and 2 and 16 galaxies with χ^2 between 2 and 3, which means a total of 139 galaxies for which the value of χ^2 is less than 3 (from the 171 galaxies that we have analyzed, *i.e.*, representing a percent of more than 80%). From this point of view we can consider that the Weyl geometric gravity model of the dark matter gives an acceptable description of the observational data of the galactic rotation curves.

Distribution of the optimal values of C_1 and C_2 . In Fig. 4.7 the distributions of the optimal values of C_1 and C_2 are presented. For better visibility we have omitted few values larger than 1.2×10^8 for C_1 , respectively larger than 3×10^8 for C_2 .

Distribution of the optimal values of $1/C_2$ and C_1/C_2^2 . In Fig. 16 the distributions of the optimal values of $1/C_2$ and C_1/C_2^2 are presented.

4.8. Correlations between the parameters of the model, and the astrophysical quantities

We proceed now to the investigation of the problem of the existence of possible correlations between the parameters of the Weyl geometric dark matter model, and between these parameters and the astrophysical quantities describing galactic properties.

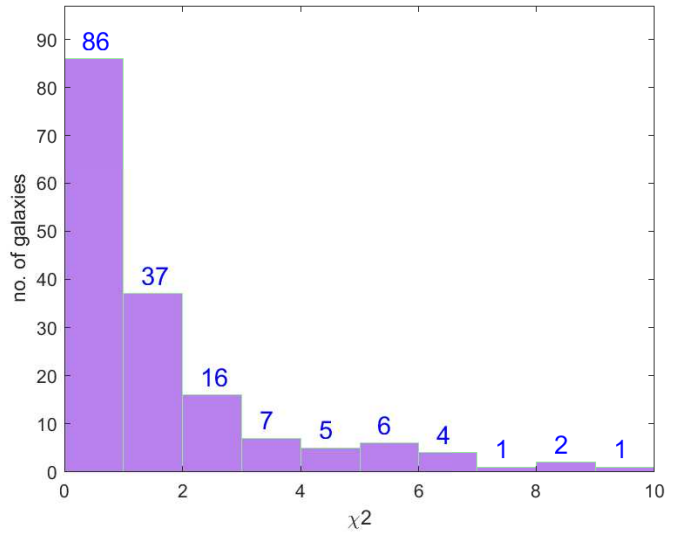


Figure 14: Histogram of the objective function χ^2 values (for $\chi^2 \leq 10$).

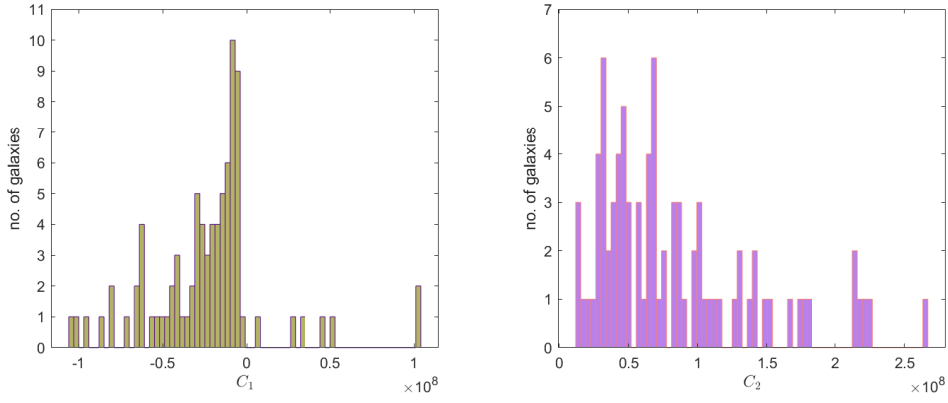


Figure 15: Histogram of the optimal values of the parameters C_1 and C_2 .

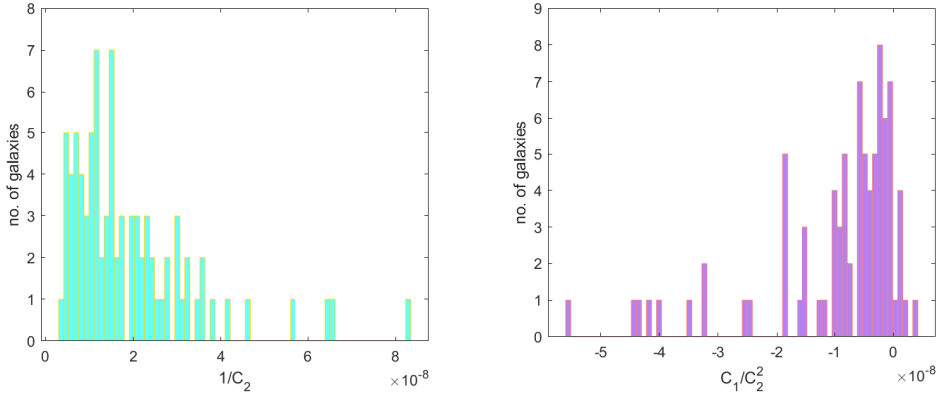


Figure 16: Histogram of the optimal values of the quantities $1/C_2$ and C_1/C_2^2 .

Correlation between C_1 and C_2 . The first plot of Fig. 17 presents the optimal values of C_2 versus the absolute values of C_1 , these values being correlated with the Pearson correlation coefficient 0.8817. The second plot shows the optimal values of C_2 versus the total luminosity of the corresponding galaxies. From the Figure one can see that they are slightly anti-correlated.

Correlation of r_g with v_{flat} and the effective radius. Fig. 18 shows a log-log plot of the optimal values of r_g versus the asymptotic value of velocity v_{flat} that indicate their medium correlation (the correlation coefficient being 0.4584). The right panel of Fig. 18 presents a semi-logarithmic plot of r_g versus the effective radius of the corresponding galaxies (again they are medium correlated with the correlation coefficient 0.4875).

Correlating C_1 with the hydrogen mass and galactic luminosity. In Fig. 19 we have represented the absolute value of the optimal values of C_1 versus the total mass of hydrogen M_{HI} , respective versus the total luminosities of the galaxies. One can see that these quantities are slightly anticorrelated.

Correlation of $1/C_2$ with v_{flat} and galactic luminosity. The left panel of Fig. 20 shows a plot of the optimal values of $1/C_2$ versus the asymptotic value of velocity v_{flat} that indicate their medium correlation (the correlation coefficient being 0.432). The right panel represents the optimal values $1/C_2$ versus the total luminosities of the galaxies (semilog plot). One can see that these quantities are slightly correlated their correlation coefficient being 0.3645.

Correlating $abs(C_1)/C_2^2$ with the hydrogen mass. In Fig. 21 we have represented the optimal quantities $abs(C_1)/C_2^2$ versus the total mass of hydrogen M_{HI} . One can see that these quantities are slightly anticorrelated the correlation coefficients being -0.3036.

5. Discussions and final remarks

Weyl geometry has experienced recently a strong revival, mostly due to its beautiful mathematical structure, and attractive physical ideas that could be implemented by using its formalism. A significant step in this direction was undertaken by Dirac [75, 76], who tried to reformulate Weyl's theory from a physical point of view, by introducing a real scalar field β

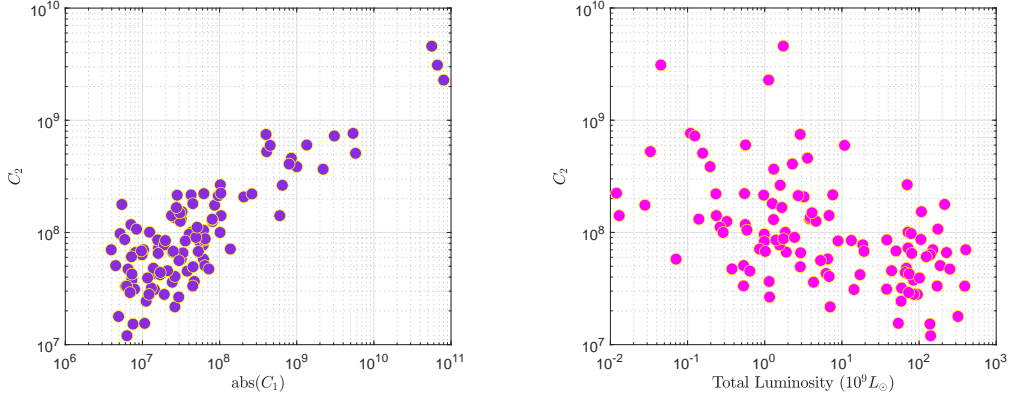


Figure 17: The optimal values of C_2 versus $abs(C_1)$ (left panel) and C_2 versus total galactic Luminosity (right panel). The correlation coefficients are 0.8817, and -0.1618, respectively.

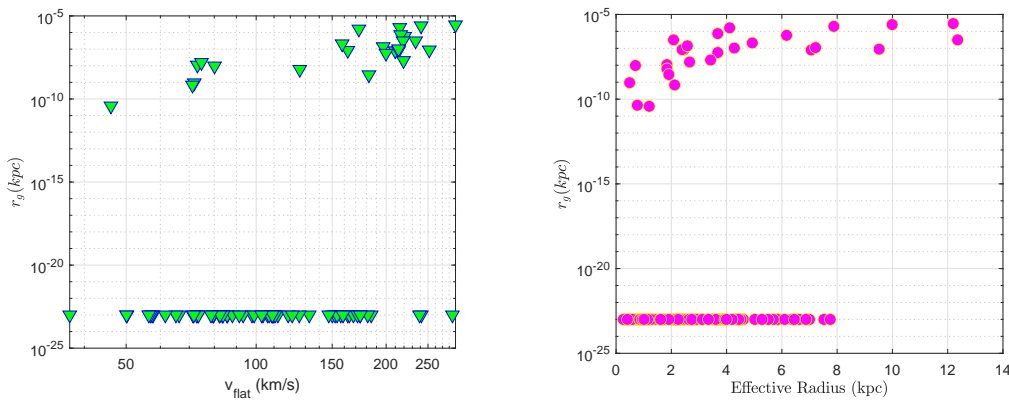


Figure 18: The optimal values of r_g versus v_{flat} (left panel), respectively r_g versus the effective radius (right panel), the correlation coefficients being 0.4584 and 0.4875.

of weight $w(\phi) = -1$. The action proposed by Dirac is conformally invariant, and in the cosmological model based on the action introduced in [76], the presence of the Dirac scalar gauge field leads to the creation of matter at the very beginning of the Universe. Moreover, in the late expansionary stages of the Universe, the Dirac scalar gauge field may represent the dark energy that triggers present accelerated cosmic expansion of the Universe. Dirac's generalization of Weyl's theory is one of the first modifications in which a new scalar degree of freedom was added to the theory in order to extend the initial vector-tensor formulation.

The idea of conformal invariance, central in Weyl geometry, is extensively used in the Conformal Cyclic Cosmology (CCC) model [77, 78], in which the basic assumption is that the Universe exists as a set of eons. Eons are geometric structures representing time oriented spacetimes. Eons possess spacelike null infinities as a result of their conformal compactification. The general physical and cosmological implications of the CCC model were studied in [79–81].

In [82] Gerard 't Hooft suggested that conformal symmetry is an exact symmetry that is spontaneously broken during the evolution of the Universe. Hence conformal symmetry could be of equal importance to the Lorentz invariance of natural laws. The

possibility of the breaking of the conformal invariance may provide a physical mechanism allowing to understand the small-scale structure of the gravitational gravity, and of the physics of the Planck scale. Based on this idea, a theory of gravity constructed from the assumption that conformal symmetry is an exact local, but spontaneously broken symmetry, was considered in [83].

In the present paper we have considered another formulation of Weyl's theory, in which the scalar degree of freedom naturally appears within the framework of the theory, and is geometric in its origin. The introduction of the auxiliary geometric scalar field significantly simplifies the mathematical formalism, and leads to the linearization of the originally quadratic action in the curvature scalar. This theory has been used to investigate various cosmological and astrophysical aspects, and in this investigation we have considered in detail the possibility that Weyl geometry could account for the observed dynamics of the galactic rotation curves.

Tentatively, to test this hypothesis, we have adopted an exact spherically symmetric solution of the Weyl geometric gravity theory as describing the geometry of the galactic halo, outside the baryonic matter distribution. We are of course aware of the limitations and simplification involved in this choice, since

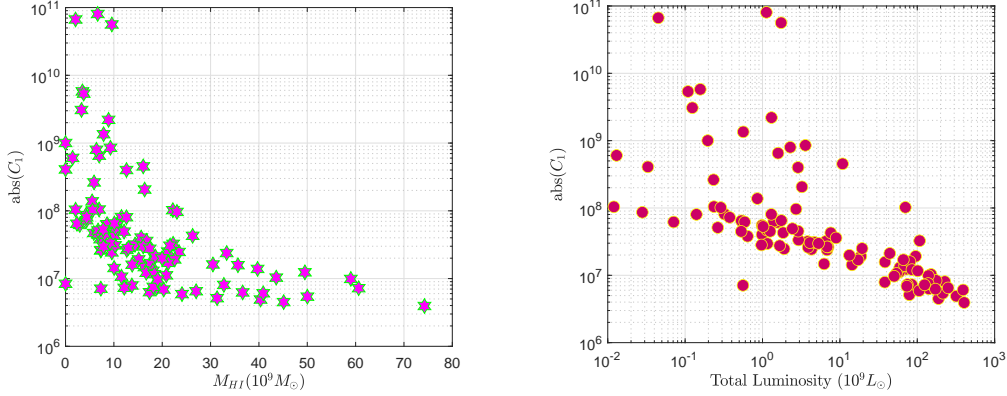


Figure 19: The optimal values of $abs(C_1)$ versus M_{HI} (left panel), respectively $abs(C_1)$ versus total galactic Luminosity (right panel).

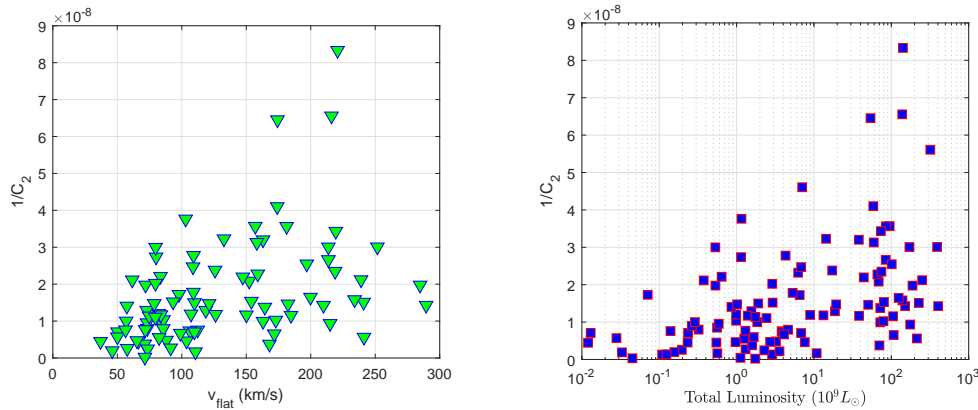


Figure 20: The optimal values of $1/C_2$ versus v_{flat} (left panel), respectively $1/C_2$ versus total galactic Luminosity (right panel), the correlation coefficients being 0.432, respectively 0.3645.

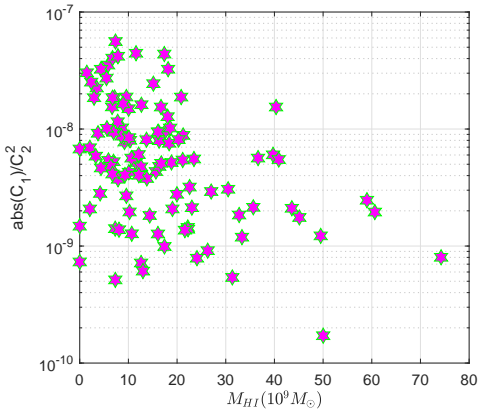


Figure 21: The optimal values of $abs(C_1)/C_2^2$ versus M_{HI} .

many other Weyl geometrical solutions may exist. However, as a first step in the direction of the Weylian description of "dark matter", this approximation may provide some hints for the viability/nonviability of such an approach. By using this exact solution we have obtained the full general relativistic expression of the tangential velocities of the massive particles in circular

stable orbits, and we have used this expression, without ante-Newtonian or post-Newtonian approximations, to compare the theoretical model with the observational data. We have compared the Weyl geometric tangential velocity expression with the rotation curves of 171 galaxies of the SPARC sample. As one can see from Fig. 14, for 86 galaxies (50% of the sample), the objective function χ^2 has values smaller than one. For a number of 123 galaxies, the objective function took values smaller than 2. There are 139 galaxies (81% of the sample) having $\chi^2 < 3$. Based on these statistical results, we may consider that the simplest possible Weyl geometric approach provides an acceptable description of the galactic rotation curves, indicating that more realistic approaches, based, for example, on the numerical solutions of the field equations, could improve the concordance between the model and the observational data.

We would also like to point out that by adding the baryonic matter contribution to the expression of the total velocity, the strict conformal symmetry of the model is broken. Adding matter in a conformally invariant way requires the consideration of the trace condition, as done, for example, in [57]. The inclusion of the matter would certainly modify the mathematical structure of the metric considered in the present study, and will open some new perspectives on the problem of the rotation curves.

One of the important requirements related to the motion of the particles in the galactic halo is that the timelike circular geodesics must be stable. Let r_0 denote the radius of a circular orbit. Let us now consider a small perturbation of the orbit r_0 of the form $r = r_0 + \delta$, where $\delta \ll r_0$ [73, 84]. By expanding $V_{eff}(r)$, as given by Eq. (42) and $\exp(\nu + \lambda)$ about $r = r_0$, it follows from Eq. (41) that the orbit perturbation satisfies the second order differential equation [84]

$$\ddot{\delta}(r) + \frac{1}{2}e^{\nu(r_0)+\lambda(r_0)}V''_{eff}(r_0)\delta(r) = 0. \quad (58)$$

Since for the present Weyl geometric gravity model the metric satisfies the condition $\nu + \lambda = 0$, the condition for the stability of the circular orbits requires that the condition $V''_{eff}(r_0) > 0$ must be satisfied [73, 84]. By assuming that $v_{ig}^2/c^2 \ll 1$, from Eq. (49) it follows that $V_{eff}(r) \approx e^{\nu(r)}$. By taking into account that $V'_{eff}(r) = v'(r)e^{\nu(r)} = (2v_{ig}^2/c^2)e^{\nu}/r$, we obtain the stability condition of the circular orbits as

$$\left| \frac{d}{dr}v_{ig}^2(r) - \frac{v_{ig}^2(r)}{r} + \frac{2v_{ig}^4}{c^2} \frac{1}{r} \right|_{r=r_0} > 0. \quad (59)$$

By neglecting the last term in the above equation, the stability condition of the circular orbits can be formulated as

$$\left. \frac{d}{dr}v_{ig}^2(r) \right|_{r=r_0} > \frac{v_{ig}^2(r_0)}{r_0}. \quad (60)$$

If the inequality (60) is true for $r_0 \in [R_b, R_{eff}]$ after dividing by $v^2(r_0)$ and integrating on this interval one obtains the condition:

$$v^2(R_{eff})/v^2(R_b) > R_{eff}/R_b. \quad (61)$$

As pointed out recently in [42], metrics of the type considered in the present investigation face the problem of their limiting tangential velocity, which, in the large radial coordinate limit tend to the speed of light, or other unrealistically high values. The impossibility of the existence of a plateau phase of the rotation curves has also been mentioned in this study. However, this raises the problem of the relation between mathematical and physical infinity. Indeed, in the limit $r \rightarrow \infty$ the tangential velocity (37) tends to c . On the other hand, the range of the radial coordinate for realistic galactic halos is of the order of the few tenths of kpcs. In this range of r a good description of the galactic rotation curves can be obtained. On the other hand, in the present model the radial dependence does appear via the dimensionless factor $r/C_2 \ll 1$. The limit to the physical infinity $r \rightarrow \infty$ would require $r \gg C_2$, when already Weyl geometric effects are negligible. This can be easily seen from Eqs. (29) and (30), which show that both the scalar field and the Weyl vector tend to zero, and we thus recover Einstein's general relativity. However, we may assume that the transition to general relativity occurs at some realistic finite astrophysical distances, $r = R$, so that for $r \geq R$, the metric is Schwarzschild, with R obtained from the relation

$$e^{\nu(R)} = e^{-\lambda(R)} = 1 - \frac{3r_g}{C_2} - \frac{r_g}{R} + \left(2 - 3\frac{r_g}{C_2}\right)\frac{R}{C_2} + \left(1 + \frac{C_1}{12} - \frac{r_g}{C_2}\right)\frac{R^2}{C_2^2} \approx 1 - \frac{R_g}{R}, \quad (62)$$

where $R_g = GM_{tot}/c^2$, with M_{tot} denoting the total galactic mass, including the contribution coming from the Weyl geometry. On the other hand we can introduce, by analogy with the Schwarzschild case, an effective dark matter gravitational radius $R_g^{(eff)}$, and an effective dark matter mass $M_{DM}^{(eff)}$, defined according to $e^{\nu(r)} = e^{-\lambda(r)} = 1 - R_g^{(eff)}(r)/r$, giving

$$R_g^{(eff)} = \frac{2GM_{DM}^{(eff)}(r)}{c^2} = r_g + \frac{3r_g}{C_2}r - \left(2 - 3\frac{3r_g}{C_2}\right)\frac{r^2}{C_2} + \left(1 + \frac{C_1}{12} - \frac{r_g}{C_2}\right)\frac{r^3}{C_2^2}, \quad (63)$$

and an effective dark matter density $\rho_{DM}^{(eff)}(r)$, defined by using the standard expression $(1/4\pi r^2)dM_{DM}^{(eff)}(r)/dr$, and which can be obtained as

$$\rho_{DM}^{(eff)}(r) = \frac{c^2}{8\pi G} \left[\frac{3r_g}{C_2} - 2\left(2 - \frac{3r_g}{C_2}\right)\frac{r}{C_2} - 3\left(1 + \frac{C_1}{12} - \frac{r_g}{C_2}\right)\frac{r^2}{C_2^2} \right] \frac{1}{r^2}. \quad (64)$$

Since the ratio r_g/C_2 has negligibly small values, and C_1 has negative values, with $abs(C_1) \gg 1$, and $r/C_2 \ll 1$, one can approximate Eq. (64) as

$$\rho_{DM}^{(eff)}(r) \approx \frac{c^2}{8\pi G} \left[\frac{1}{4} \frac{C_1}{C_2^2} - \frac{4}{C_2 r} \right]. \quad (65)$$

By taking now into account the expressions (29) and (30) of the scalar field and of the Weyl vector, after eliminating the constants we obtain the energy density of the effective Weyl geometric dark matter in the form

$$\rho_{DM}^{(eff)}(r) \approx \frac{c^2}{32\pi G} \left[\Phi(r) + 8\alpha \frac{\omega_1(r)}{r} \right]. \quad (66)$$

Eq. (66) is valid in a region of space-time where the variation of the scalar field and of the Weyl vector is very slow. Hence, the effective physical properties of the galactic dark matter halos, including their density and mass distribution is indeed determined by the geometrical degrees of freedom that characterize the Weyl geometry effects at the galactic level.

The results of this investigation have provided some evidence for the potential of the simplest Weyl geometric gravity model as an alternative to the dark matter paradigm. Further, and detailed investigations in this field are certainly necessary to convincingly confirm, or infirm, the validity, and astrophysical relevance of this approach. Our results are thus only a first step in developing the theoretical and observational tools necessary to test the presence/absence of Weyl geometrical effects at the galactic and met-galactic levels.

Acknowledgments

The work of TH is supported by a grant of the Romanian Ministry of Education and Research, CNCS-UEFISCDI, project number PN-III-P4-ID-PCE-2020-2255 (PNCDI III).

References

- [1] Planck Collaboration, N. Aghanim, A. et al., *Planck* 2018 results: VI. Cosmological parameters, *Astron. Astrophys.* 641 (2020) A6. doi:10.1051/0004-6361/201833910.
- [2] L. V. Sales, A. Wetzel, A. Fattahi, Baryonic solutions and challenges for cosmological models of dwarf galaxies, *Nature Astronomy* 6 (8) (2022) 897–910. doi:10.1038/s41550-022-01689-w.
- [3] J. F. Navarro, C. S. Frenk, S. D. M. White, The Structure of Cold Dark Matter Halos, *Astrophys. J.* 462 (1996) 563. doi:10.1086/177173.
- [4] S.-H. Oh, W. De Blok, E. Brinks, F. Walter, R. C. Kennicutt, Dark and luminous matter in THINGS dwarf galaxies, *Astron. J.* 141 (6) (2011) 193. doi:10.1088/0004-6256/141/6/193.
- [5] C. Boehmer, T. Harko, Can dark matter be a Bose-Einstein condensate?, *JCAP* 2007 (06) (2007) 025. doi:10.1088/1475-7516/2007/06/025.
- [6] T. Harko, Bose-Einstein condensation of dark matter solves the core/cusp problem, *JCAP* 2011 (05) (2011) 022. doi:10.1088/1475-7516/2011/05/022.
- [7] M. Crăciun, T. Harko, Testing Bose-Einstein condensate dark matter models with the SPARC galactic rotation curves data, *Eur. Phys. J. C* 80 (8) (2020) 735. doi:10.1140/epjc/s10052-020-8272-4.
- [8] M. Milgrom, A modification of the Newtonian dynamics-implications for galaxies, *Astrophys. J.* 270 (1983) 371–383. doi:10.1086/161131.
- [9] M. K. Mak, T. Harko, Can the galactic rotation curves be explained in brane world models?, *Phys. Rev. D* 70 (2004) 024010. doi:10.1103/PhysRevD.70.024010.
- [10] T. Harko, K. S. Cheng, Virial theorem and the dynamics of clusters of galaxies in the brane world models, *Phys. Rev. D* 76 (2007) 044013. doi:10.1103/PhysRevD.76.044013.
- [11] O. Bertolami, C. G. Böhmer, T. Harko, F. S. N. Lobo, Extra force in $f(r)$ modified theories of gravity, *Phys. Rev. D* 75 (2007) 104016. doi:10.1103/PhysRevD.75.104016.
- [12] C. G. Böhmer, T. Harko, F. S. Lobo, The generalized virial theorem in $f(r)$ gravity, *JCAP* 2008 (03) (2008) 024. doi:10.1088/1475-7516/2008/03/024.
- [13] C. G. Böhmer, T. Harko, F. S. Lobo, Dark matter as a geometric effect in $f(r)$ gravity, *Astroparticle Physics* 29 (6) (2008) 386–392. doi:https://doi.org/10.1016/j.astropartphys.2008.04.003.
- [14] H. Sepangi, S. Shahidi, Virial mass in DGP brane cosmology, *Class. Quantum Gravity* 26 (18) (2009) 185010. doi:10.1088/0264-9381/26/18/185010.
- [15] A. S. Sefiedgar, K. Atazadeh, H. R. Sepangi, Generalized virial theorem in Palatini $f(\mathcal{R})$ gravity, *Phys. Rev. D* 80 (2009) 064010. doi:10.1103/PhysRevD.80.064010.
- [16] T. Harko, F. S. N. Lobo, S. Nojiri, S. D. Odintsov, $f(r, t)$ gravity, *Phys. Rev. D* 84 (2011) 024020. doi:10.1103/PhysRevD.84.024020.
- [17] A. S. Sefiedgar, Z. Haghani, H. R. Sepangi, Brane- $f(r)$ gravity and dark matter, *Phys. Rev. D* 85 (2012) 064012. doi:10.1103/PhysRevD.85.064012.
- [18] O. Bertolami, P. Frazão, J. Páramos, Mimicking dark matter in galaxy clusters through a nonminimal gravitational coupling with matter, *Phys. Rev. D* 86 (2012) 044034. doi:10.1103/PhysRevD.86.044034.
- [19] L. Lombriser, F. Schmidt, T. Baldauf, R. Mandelbaum, U. Seljak, R. E. Smith, Cluster density profiles as a test of modified gravity, *Phys. Rev. D* 85 (2012) 102001. doi:10.1103/PhysRevD.85.102001.
- [20] S. Capozziello, T. Harko, T. S. Koivisto, F. S. Lobo, G. J. Olmo, The virial theorem and the dark matter problem in hybrid metric-Palatini gravity, *JCAP* 2013 (07) (2013) 024. doi:10.1088/1475-7516/2013/07/024.
- [21] T. Harko, F. S. Lobo, M. Mak, S. V. Sushkov, Dark matter density profile and galactic metric in Eddington-inspired Born-Infeld gravity, *Mod. Phys. Lett.* 29 (09) (2014) 1450049. doi:10.1142/S0217732314500497.
- [22] R. Myrzakulov, L. Sebastiani, S. Vagnozzi, S. Zerbini, Static spherically symmetric solutions in mimetic gravity: rotation curves and wormholes, *Class Quantum Gravity* 33 (12) (2016) 125005. doi:10.1088/0264-9381/33/12/125005.
- [23] L. Sebastiani, S. Vagnozzi, R. Myrzakulov, et al., Mimetic gravity: a review of recent developments and applications to cosmology and astrophysics, *Adv. High Energy Phys.* 2017 (2017). doi:10.1155/2017/3156915.
- [24] S. Vagnozzi, Recovering a MOND-like acceleration law in mimetic gravity, *Class. Quantum Gravity* 34 (18) (2017) 185006. doi:10.1088/1361-6382/aa838b.
- [25] T. Harko, F. S. Lobo, Extensions of $f(R)$ Gravity: Curvature-Matter Couplings and Hybrid Metric-Palatini Theory, Vol. 1, Cambridge University Press, 2018. doi:10.1017/9781108645683.
- [26] J. M. Overduin, P. S. Wesson, Dark matter and background light, *Phys. Rep.* 402 (5-6) (2004) 267–406. doi:10.1016/j.physrep.2004.07.006.
- [27] H. Weyl, Gravitation und elektrizität, *Sitzungsberichte der Königlich Preußischen Akademie der Wissenschaften zu Berlin* (1918) 465–480.
- [28] H. Weyl, *Space, Time, Matter*, Dover, New York, 1952.
- [29] E. Scholz, The unexpected resurgence of Weyl geometry in late 20th-century physics, *arXiv:1703.03187* (2017). doi:10.48550/arXiv.1703.03187.
- [30] G. K. Karananas, A. Monin, Weyl vs. conformal, *Phys. Lett. B* 757 (2016) 257–260. doi:https://doi.org/10.1016/j.physletb.2016.04.001.
- [31] P. D. Mannheim, D. Kazanas, Exact vacuum solution to conformal Weyl gravity and galactic rotation curves, *Astrophys. J.* 342 (1989) 635–638.
- [32] P. D. Mannheim, Open questions in classical gravity, *Found. Phys.* 24 (1994) 487–511. doi:10.1007/BF02058060.
- [33] P. D. Mannheim, Local and global gravity, *Found. Phys.* 26 (1996) 1683–1709. doi:10.1007/BF02282129.
- [34] P. D. Mannheim, Attractive and repulsive gravity, *Found. Phys.* 30 (2000) 709–746. doi:10.1023/A:1003737011054.
- [35] P. D. Mannheim, Solution to the ghost problem in fourth order derivative theories, *Found. Phys.* 37 (2007) 532–571. doi:10.1007/s10701-007-9119-7.
- [36] P. D. Mannheim, Making the case for conformal gravity, *Found. Phys.* 42 (2012) 388–420. doi:10.1007/s10701-011-9608-6.
- [37] P. D. Mannheim, J. G. O’Brien, Impact of a global quadratic potential on galactic rotation curves, *Phys. Rev. Lett.* 106 (2011) 121101. doi:10.1103/PhysRevLett.106.121101.
- [38] P. D. Mannheim, J. G. O’Brien, Fitting galactic rotation curves with conformal gravity and a global quadratic potential, *Phys. Rev. D* 85 (2012) 124020. doi:10.1103/PhysRevD.85.124020.
- [39] J. G. O’Brien, P. D. Mannheim, Fitting dwarf galaxy rotation curves with conformal gravity, *Mon. Not. R. Astron. Soc.* 421 (2) (2012) 1273–1282. doi:10.1111/j.1365-2966.2011.20386.x.
- [40] J. G. O’Brien, T. L. Chiarelli, P. D. Mannheim, Universal properties of galactic rotation curves and a first principles derivation of the Tully–Fisher relation, *Phys. Lett. B* 782 (2018) 433–439. doi:10.1016/j.physletb.2018.05.060.
- [41] D. Cemsinan, K. Oğuzhan, Y. Barış, Flat galactic rotation curves from geometry in Weyl gravity, *Astrophys. Space Sci.* 365 (3) (2020). doi:10.1007/s10509-020-03764-y.
- [42] M. Hobson, A. Lasenby, Conformally-rescaled Schwarzschild metrics do not predict flat galaxy rotation curves, *Eur. Phys. J. C* 82 (7) (2022) 585. doi:10.1140/epjc/s10052-022-10531-6.
- [43] D. M. Ghilencea, Spontaneous breaking of Weyl quadratic gravity to Einstein action and Higgs potential, *JHEP* 2019 (3) (2019) 1–15. doi:10.1007/JHEP03(2019)049.
- [44] D. M. Ghilencea, H. M. Lee, Weyl gauge symmetry and its spontaneous breaking in the standard model and inflation, *Phys. Rev. D* 99 (2019) 115007. doi:10.1103/PhysRevD.99.115007.
- [45] D. M. Ghilencea, Weyl r^2 inflation with an emergent Planck scale, *JHEP* 2019 (10) (2019) 1–15. doi:10.1007/JHEP10(2019)209.
- [46] D. M. Ghilencea, Stueckelberg breaking of Weyl conformal geometry and applications to gravity, *Phys. Rev. D* 101 (2020) 045010. doi:10.1103/PhysRevD.101.045010.
- [47] D. M. Ghilencea, Palatini quadratic gravity: spontaneous breaking of gauged scale symmetry and inflation, *Eur. Phys. J. C* 80 (12) (2020) 1147. doi:10.1140/epjc/s10052-020-08722-0.
- [48] D. M. Ghilencea, Gauging scale symmetry and inflation: Weyl versus Palatini gravity, *Eur. Phys. J. C* 81 (6) (2021) 510. doi:10.1140/epjc/s10052-021-09226-1.
- [49] D. M. Ghilencea, Standard model in Weyl conformal geometry, *Eur. Phys. J. C* 82 (1) (2022) 23. doi:10.1140/epjc/s10052-021-09887-y.
- [50] D. M. Ghilencea, Non-metric geometry as the origin of mass in

- gauge theories of scale invariance, *Eur. Phys. J. C* 83 (2) (2023) 176. doi:10.1140/epjc/s10052-023-11237-z.
- [51] M. Weißwange, D. M. Ghilencea, D. Stöckinger, Quantum scale invariance in gauge theories and applications to muon production, *Phys. Rev. D* 107 (2023) 085008. doi:10.1103/PhysRevD.107.085008.
- [52] D. M. Ghilencea, C. T. Hill, Renormalization group for nonminimal $\phi^2 r$ couplings and gravitational contact interactions, *Phys. Rev. D* 107 (2023) 085013. doi:10.1103/PhysRevD.107.085013.
- [53] T. Harko, N. Myrzakulov, R. Myrzakulov, S. Shahidi, Non-minimal geometry–matter couplings in Weyl–Cartan space–times: $f(r, t, q, tm)$ gravity, *Phys. Dark Universe* 34 (2021) 100886. doi:10.1016/j.dark.2021.100886.
- [54] T. Harko, S. Shahidi, Coupling matter and curvature in Weyl geometry: conformally invariant $f(r, l_m)$ gravity, *Eur. Phys. J. C* 82 (3) (2022) 219.
- [55] J.-Z. Yang, S. Shahidi, T. Harko, Black hole solutions in the quadratic Weyl conformal geometric theory of gravity, *Eur. Phys. J. C* 82 (12) (2022) 1171. doi:10.1140/epjc/s10052-022-11131-0.
- [56] P. Burikham, T. Harko, K. Pimsamarn, S. Shahidi, Dark matter as a Weyl geometric effect, *Phys. Rev. D* 107 (2023) 064008. doi:10.1103/PhysRevD.107.064008.
- [57] Z. Haghani, T. Harko, Compact stellar structures in Weyl geometric gravity, *Phys. Rev. D* 107 (2023) 064068. doi:10.1103/PhysRevD.107.064068.
- [58] M. A. Oancea, T. Harko, Weyl geometric effects on the propagation of light in gravitational fields, arXiv preprint arXiv:2305.01313 (2023). doi:10.48550/arXiv.2305.01313.
- [59] F. Lelli, S. S. McGaugh, J. M. Schombert, M. S. Pawlowski, The relation between stellar and dynamical surface densities in the central regions of disk galaxies, *Astrophys. J. Lett.* 827 (1) (2016) L19. doi:10.3847/2041-8205/827/1/L19.
- [60] F. Lelli, S. S. McGaugh, J. M. Schombert, SPARC: Mass models for 175 disk galaxies with Spitzer photometry and accurate rotation curves, *Astron. J.* 152 (6) (2016) 157. doi:10.3847/0004-6256/152/6/157.
- [61] S. S. McGaugh, F. Lelli, J. M. Schombert, Radial acceleration relation in rotationally supported galaxies, *Phys. Rev. Lett.* 117 (2016) 201101. doi:10.1103/PhysRevLett.117.201101.
- [62] T. Bernal, L. M. Fernández-Hernández, T. Matos, M. A. Rodríguez-Meza, Rotation curves of high-resolution LSB and SPARC galaxies with fuzzy and multistate (ultralight boson) scalar field dark matter, *Mon. Not. R. Astron. Soc.* 475 (2) (2017) 1447–1468. doi:10.1093/mnras/stx3208.
- [63] M. H. Chan, H. K. Hui, Testing the cubic Galileon gravity model by the Milky Way rotation curve and SPARC data, *Astrophys. J.* 856 (2) (2018) 177. doi:10.3847/1538-4357/aab3e6.
- [64] P. Li, F. Lelli, S. McGaugh, J. Schombert, Fitting the radial acceleration relation to individual SPARC galaxies, *Astron. Astrophys.* 615 (2018) A3. doi:10.1051/0004-6361/201732547.
- [65] J. Petersen, F. Lelli, A first attempt to differentiate between modified gravity and modified inertia with galaxy rotation curves, *Astron. Astrophys.* 636 (2020) A56. doi:10.1051/0004-6361/201936964.
- [66] P. Li, F. Lelli, S. McGaugh, J. Schombert, A comprehensive catalog of dark matter halo models for SPARC galaxies, *Astrophys. J., Suppl. Ser.* 247 (1) (2020) 31. doi:10.3847/1538-4365/ab700e.
- [67] M. H. Chan, C. F. Yeung, Model-independent constraints on ultralight dark matter from the SPARC data, *Astrophys. J.* 913 (1) (2021) 25. doi:10.3847/1538-4357/abf42f.
- [68] N. Bar, K. Blum, C. Sun, Galactic rotation curves versus ultralight dark matter: A systematic comparison with SPARC data, *Phys. Rev. D* 105 (2022) 083015. doi:10.1103/PhysRevD.105.083015.
- [69] L. Street, N. Y. Gnedin, L. C. R. Wijewardhana, Testing multiflavored ultralight dark matter models with SPARC, *Phys. Rev. D* 106 (2022) 043007. doi:10.1103/PhysRevD.106.043007.
- [70] M. Khelashvili, A. Rudakovskiy, S. Hossenfelder, Dark matter profiles of SPARC galaxies: a challenge to fuzzy dark matter, *Mon. Not. R. Astron. Soc.* 523 (3) (2023) 3393–3405. doi:10.1093/mnras/stad1595.
- [71] Landau, E. M. Lifshitz, *The Classical Theory of Fields*, Butterworths–Heinemann, London, 1973.
- [72] S. Panpanich, P. Burikham, Fitting rotation curves of galaxies by de Rham-Gabadadze-Tolley massive gravity, *Phys. Rev. D* 98 (2018) 064008. doi:10.1103/PhysRevD.98.064008.
- [73] K. Lake, Galactic potentials, *Phys. Rev. Lett.* 92 (2004) 051101. doi:10.1103/PhysRevLett.92.051101.
- [74] Z. Ugray, L. Lasdon, J. Plummer, F. Glover, J. Kelly, R. Martí, Scatter search and local NLP solvers: A multistart framework for global optimization, *INFORMS Journal on computing* 19 (3) (2007) 328–340. doi:10.1287/ijoc.1060.0175.
- [75] P. A. M. Dirac, Long range forces and broken symmetries, *Proceedings of the Royal Society of London. A. Mathematical and Physical Sciences* 333 (1595) (1973) 403–418. doi:10.1098/rspa.1973.0070.
- [76] P. A. M. Dirac, Cosmological models and the large numbers hypothesis, *Proceedings of the Royal Society of London. A. Mathematical and Physical Sciences* 338 (1615) (1974) 439–446. doi:10.1098/rspa.1974.0095.
- [77] R. Penrose, *Cycles of time: an extraordinary new view of the universe*, Random House, 2010.
- [78] V. G. Gurzadyan, R. Penrose, On CCC-predicted concentric low-variance circles in the CMB sky, *Eur. Phys. J. Plus* 128 (2013) 1–17. doi:10.1140/epjp/i2013-13022-4.
- [79] I. Bars, P. J. Steinhardt, N. Turok, Cyclic cosmology, conformal symmetry and the metastability of the Higgs, *Phys. Lett. B*.
- [80] R. Penrose, On the gravitization of quantum mechanics 2: Conformal cyclic cosmology, *Found. Phys.* 44 (2014) 873–890. doi:10.1007/s10701-013-9763-z.
- [81] P. Tod, The equations of Conformal Cyclic Cosmology, *Gen. Relativ. Gravit.* 47 (2015) 1–13. doi:10.1007/s10714-015-1859-7.
- [82] G. 't Hooft, Local conformal symmetry: The missing symmetry component for space and time, *Int. J. Mod. Phys. D* 24 (12) (2015) 1543001. doi:10.1142/S0218271815430014.
- [83] G. 't Hooft, Singularities, horizons, firewalls, and local conformal symmetry, in: *2nd Karl Schwarzschild Meeting on Gravitational Physics*, Springer, 2018, pp. 1–12.
- [84] T. Harko, K. S. Cheng, Galactric metric, dark radiation, dark pressure, and gravitational lensing in brane world models, *Astrophys. J.* 636 (1) (2006) 8. doi:10.1086/498141.